CENTER FOR ASTROPHYSICS
HARVARD & SMITHSONIAN

Intensity Interferometry with Cherenkov Telescopes

Michael Daniel

<michael.daniel@cfa.harvard.edu>

9th May, 2019

The motivation for sub-milliarcsecond astronomy

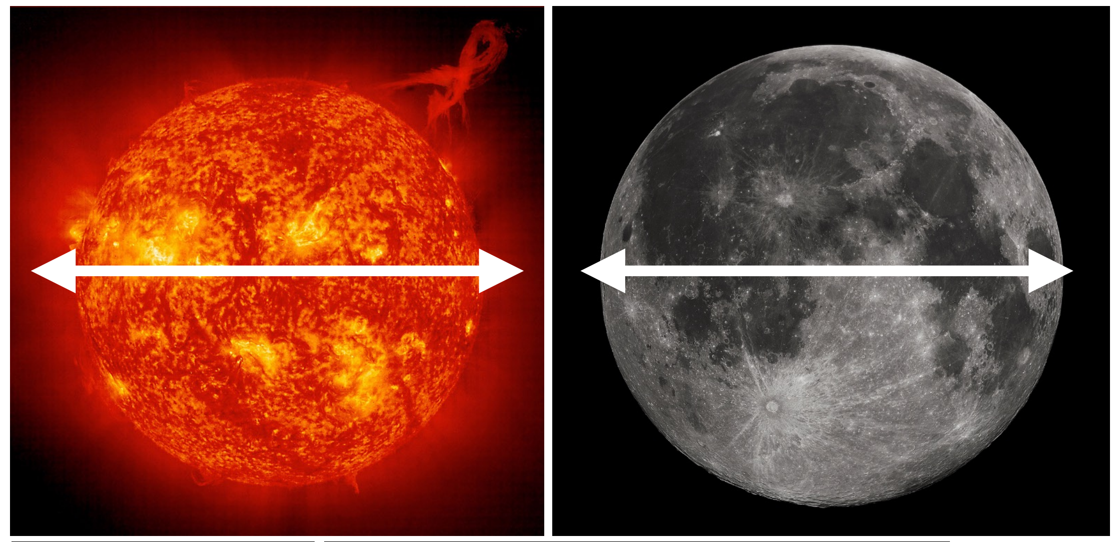

Sun, Moon
~30arcmin

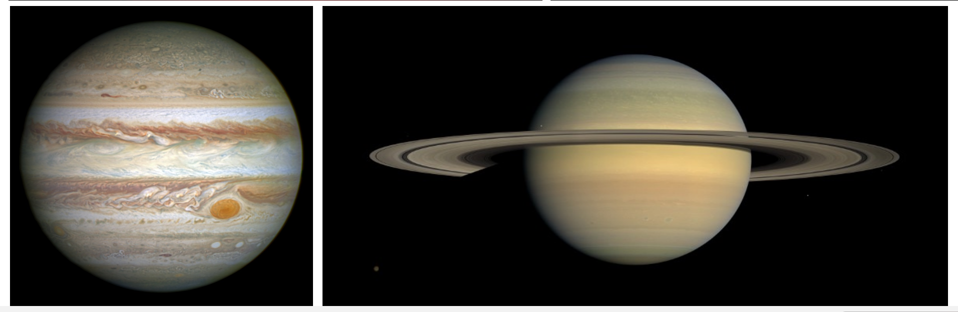

Local planets
~30arcsec

Largest stars
~30mas

Typical bright stars
~1mas

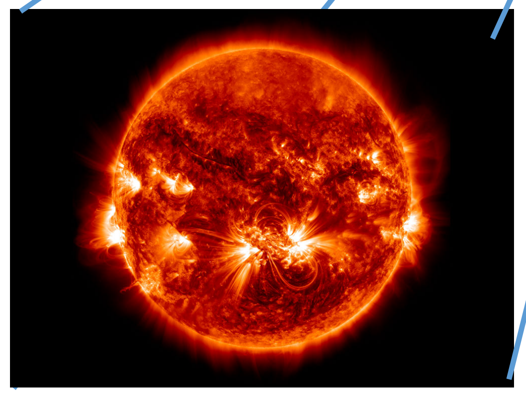

$$\theta \sim \lambda/d$$

Remember the interferometer is "blind" to any scale that does not have a baseline measurement

Many stars only become resolved surfaces for baselines 100-1000m

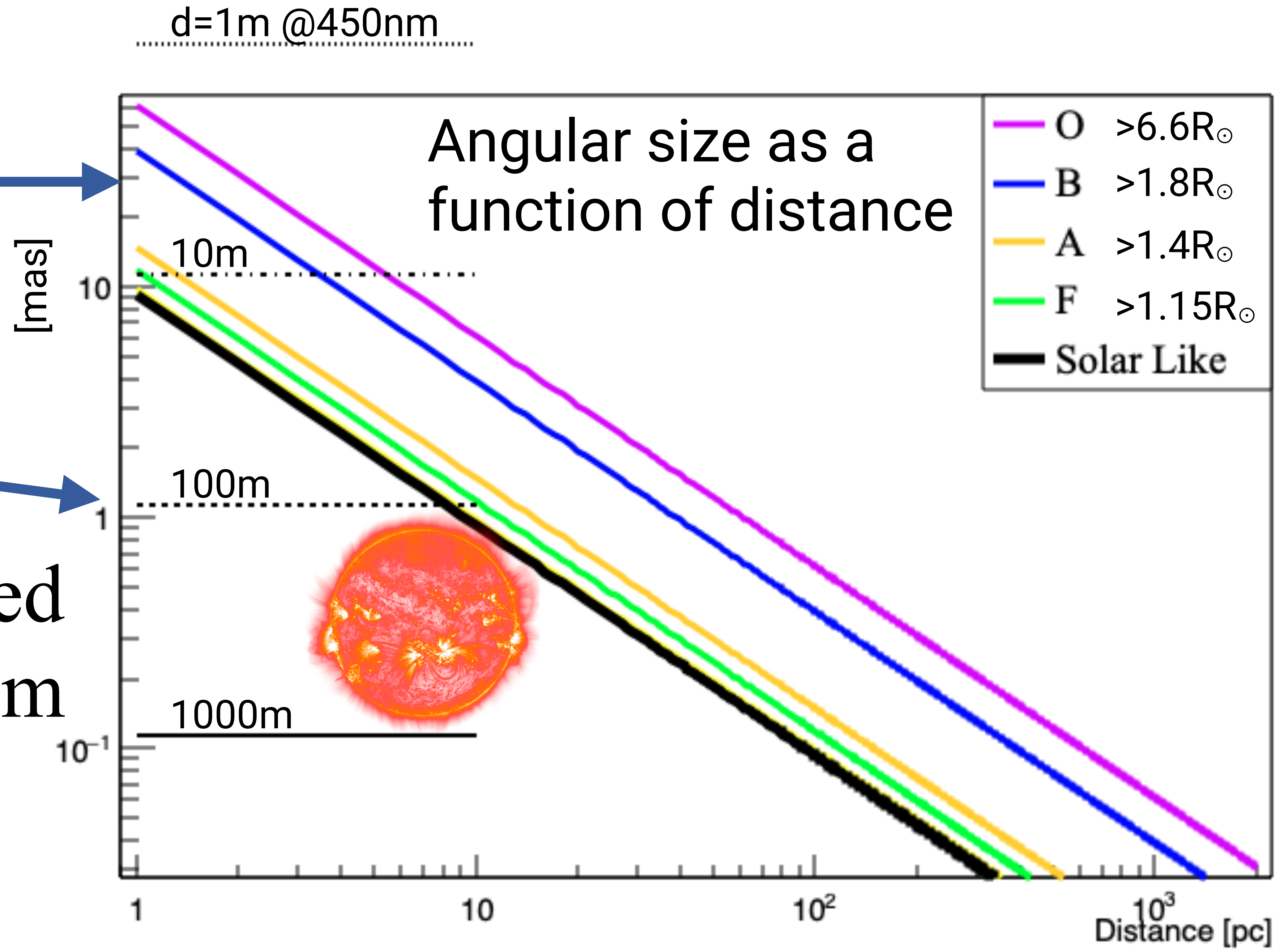

A little theory

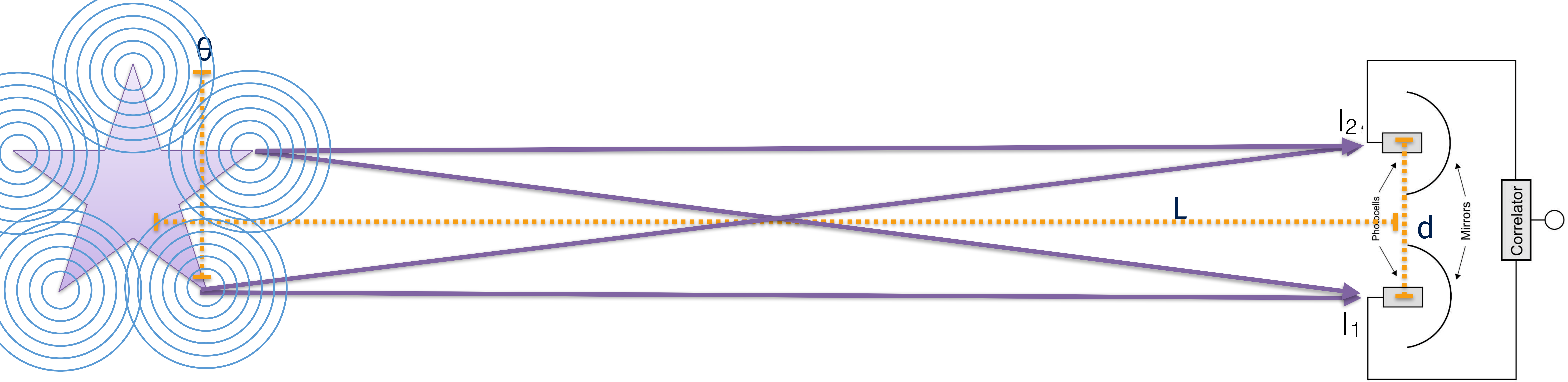

An extended body of angular diameter θ consisting of many incoherently emitting sources produces a speckled pattern at the observer of typical size λ/θ

A pair of observers separated by a distance ≪λ/θ are in the same speckle and ∴ see the same intensity fluctuations.

Observers separated by ≫λ/θ are likely to be in different speckles and see fluctuations with less or no correlation.

Measuring the scale at which the signals become de-correlated gives a measure of the angular size of the emission region.

$$\langle I_1(t)I_2(t)\rangle = \langle I_1(t)\rangle\langle I_2(t)\rangle(1 + |\Gamma_{12}|^2)$$

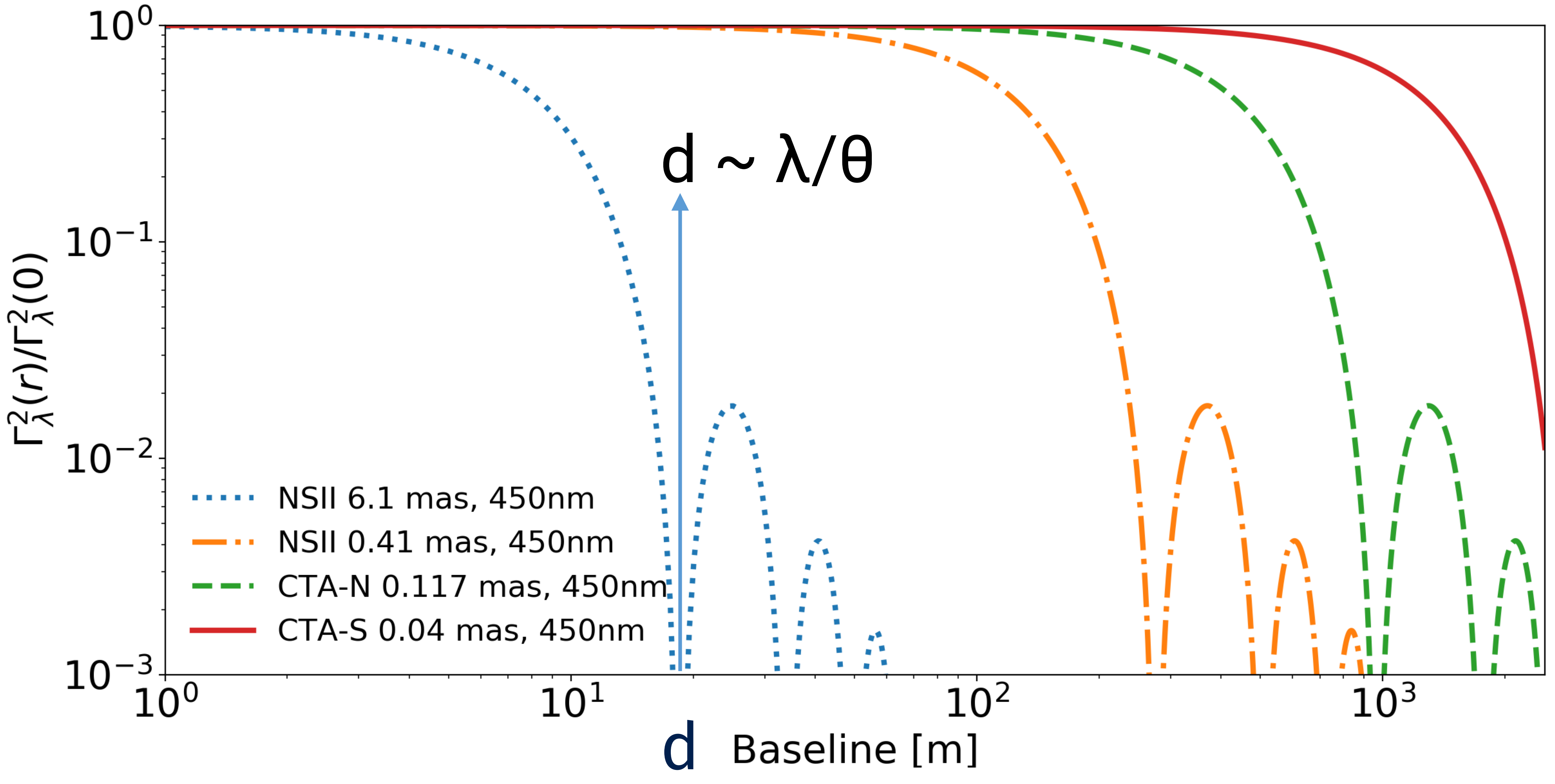

Second order time coherence $g^{(2)}$ & Fourier image plane

Van Cittert-Zernike Theorem $g^{(1)}(u,v,0) = \iint I(l,m) e^{-2\pi(lu+mv)} dl dm$

image size & brightness distribution

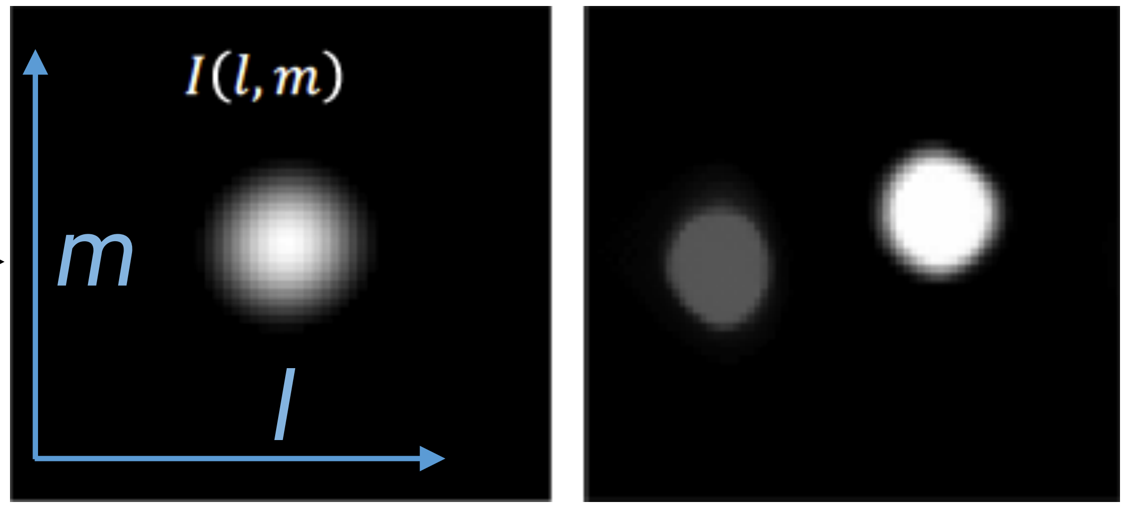

Matthews, Kieda & LeBohec *JMOp* **65**, 1336 (2018).

$$\frac{< I_1 I_2 >}{< I_1 > < I_2 >} = g^{(2)}(u,v,t) = 1 + |g^{(1)}(u,v,t)|^2$$

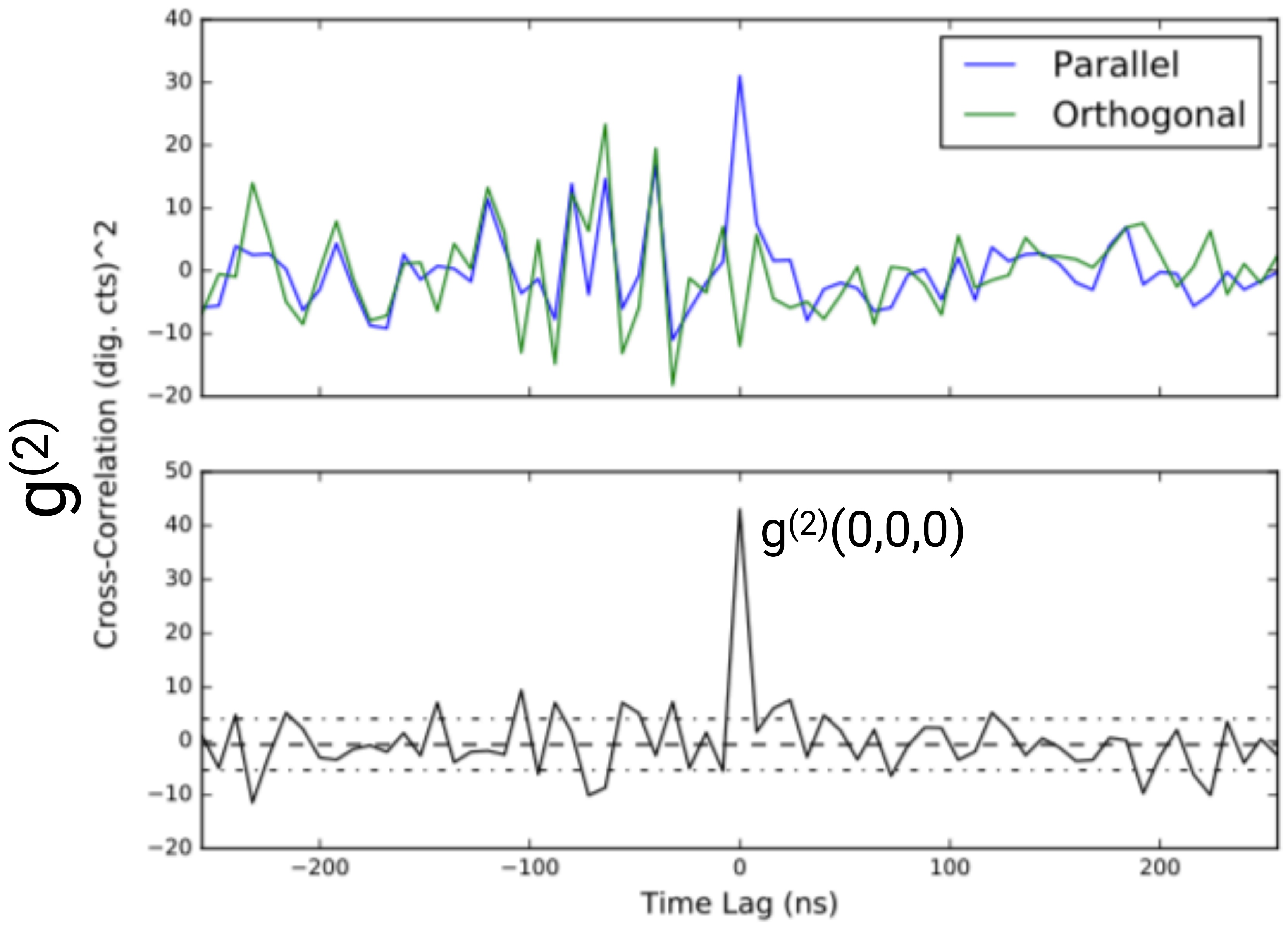

$g^{(2)}(0,0,0) = 1 + \varepsilon \sim 1 + 10^{-4}$ -> small non-Gaussian fluctuations requires large photon statistics, i.e. large collecting surfaces

Intensity fluctuations lose the phase information, but this can be recovered / compensated for

- e.g. Cauchy-Riemann algorithm Nuñez et al. MNRAS (2012).
- e.g. three point intensity correlations Nuñez & Domiciano de Souza MNRAS (2015).

A little history

* NB, also later used as a Cherenkov telescope, Grindlay et al. (1975).

Narrabri Stellar Intensity Interferometer (NSII)

- 2x 6.5m dishes on a 188m diameter circular track
  - large mirror surface, with simple optics looks like an IACT.

- Measured angular diameter of 32 stars $-2 < m_V < 3$

Hanbury Brown, Davis & Allen *MNRAS* **167**, 121 (1974)

- Directly measured limb darkening of Sirius

Hanbury Brown, Davis Lake & Thompson *MNRAS* **167**, 475 (1974)

- Multiple stars & spectroscopic binaries (e.g. Spica/α Vir)

Herbison-Evans, Hanbury Brown, Davis & Allen *MNRAS* **151**, 161 (1971)

- Emission line regions around a star (γ Velorum)

Herbison-Evans, Hanbury Brown, Davis & Allen *MNRAS* **148**, 103 (1970)

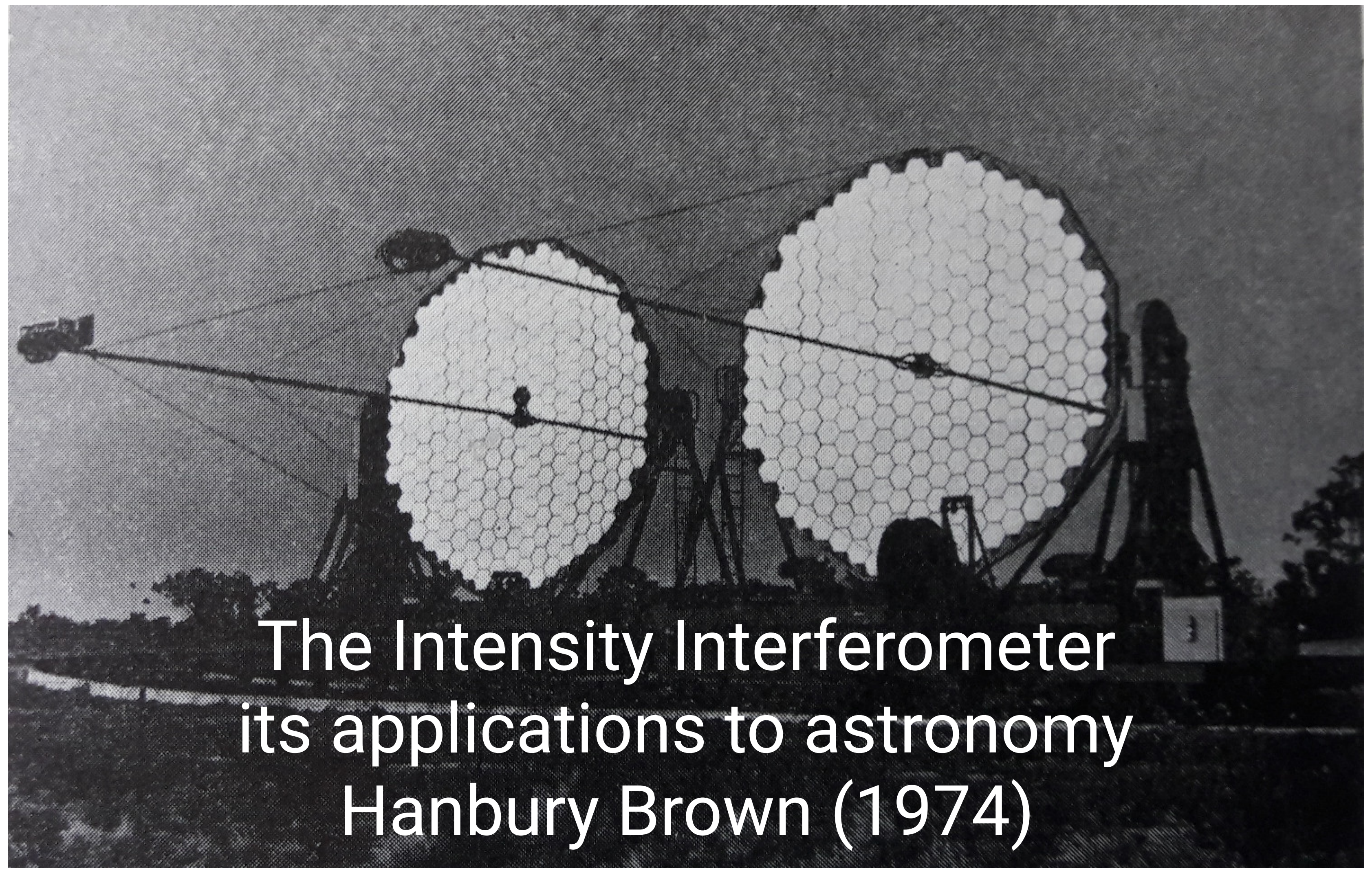

The Intensity Interferometer its applications to astronomy Hanbury Brown (1974)

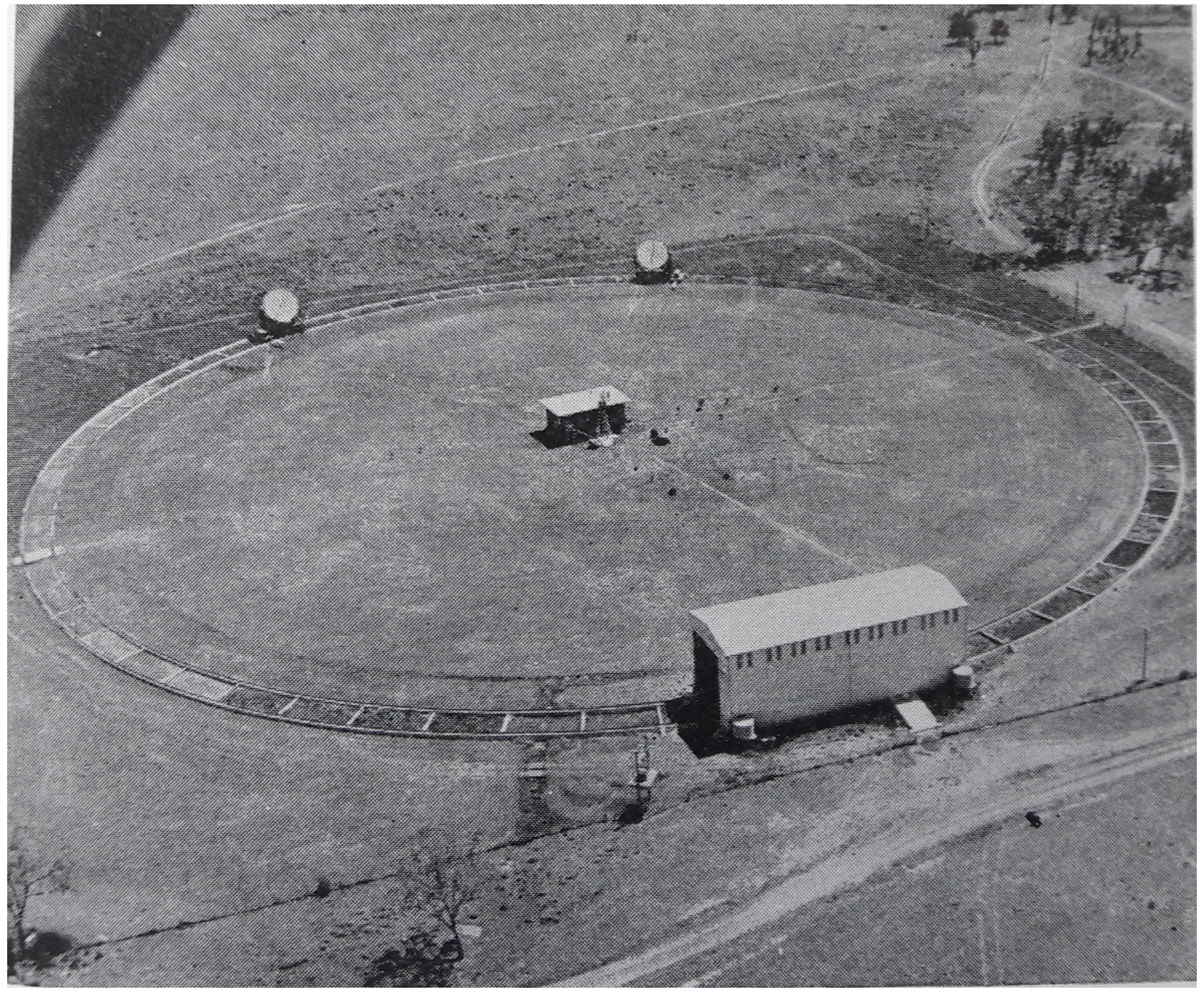

A lot of science…

in a short space of time

- angular diameters
- limb darkening
- rapid rotators
- binary systems
- emission line regions
- star spots
- …

see also, e.g.

Hanbury Brown (1974)
Barbieri et al Astro2010 paper 61, arXiv:0903.0062
Dravins et al *NewAR* **56**, 143 (2012).
Dravins et al *APh* **43**, 331 (2013).
Kieda et al Astro2020 paper ID 304 (2019).

The first dimension — angular size of stars - uniform disc

The larger the baselines, the smaller the detail we can see

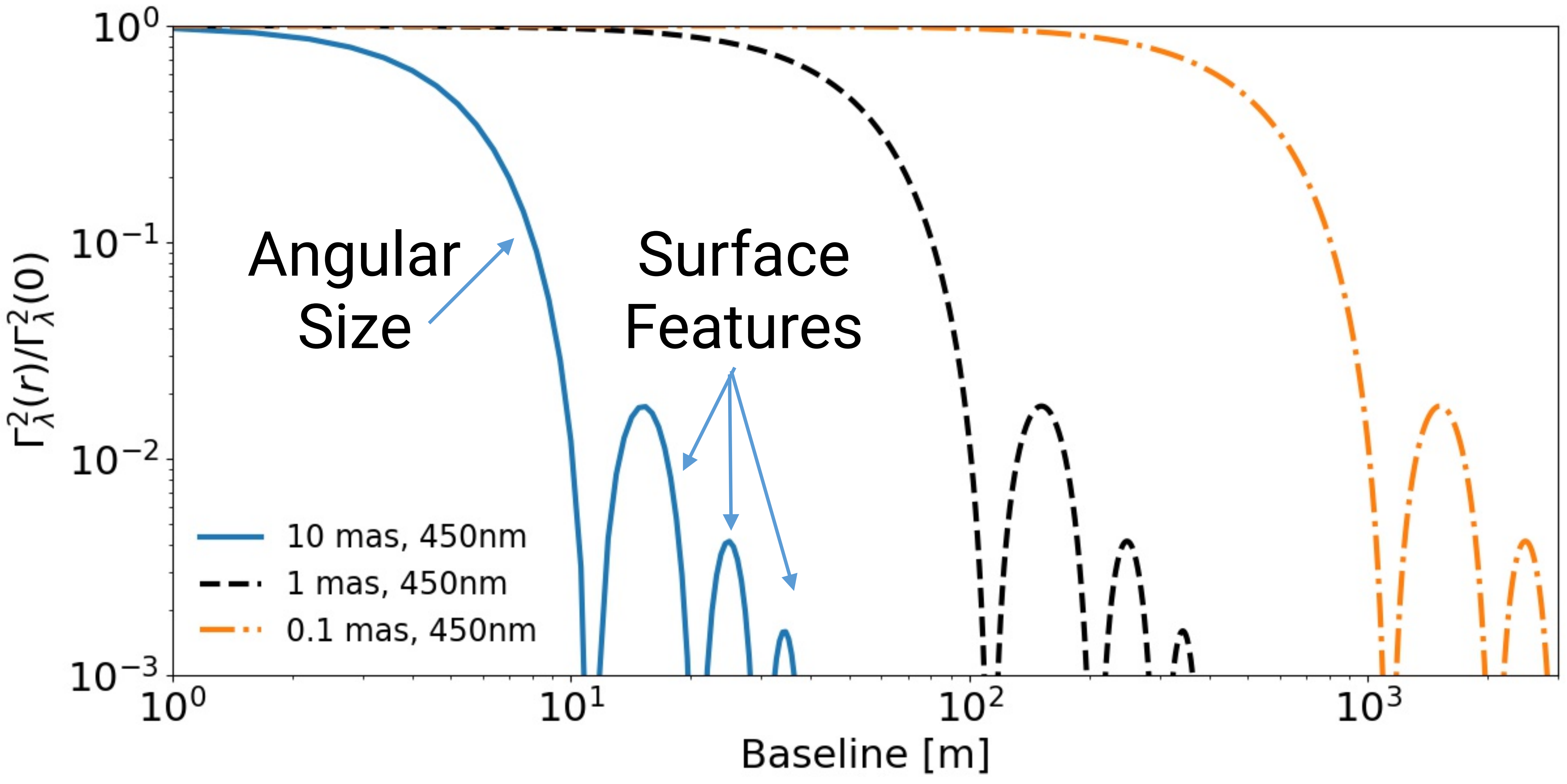

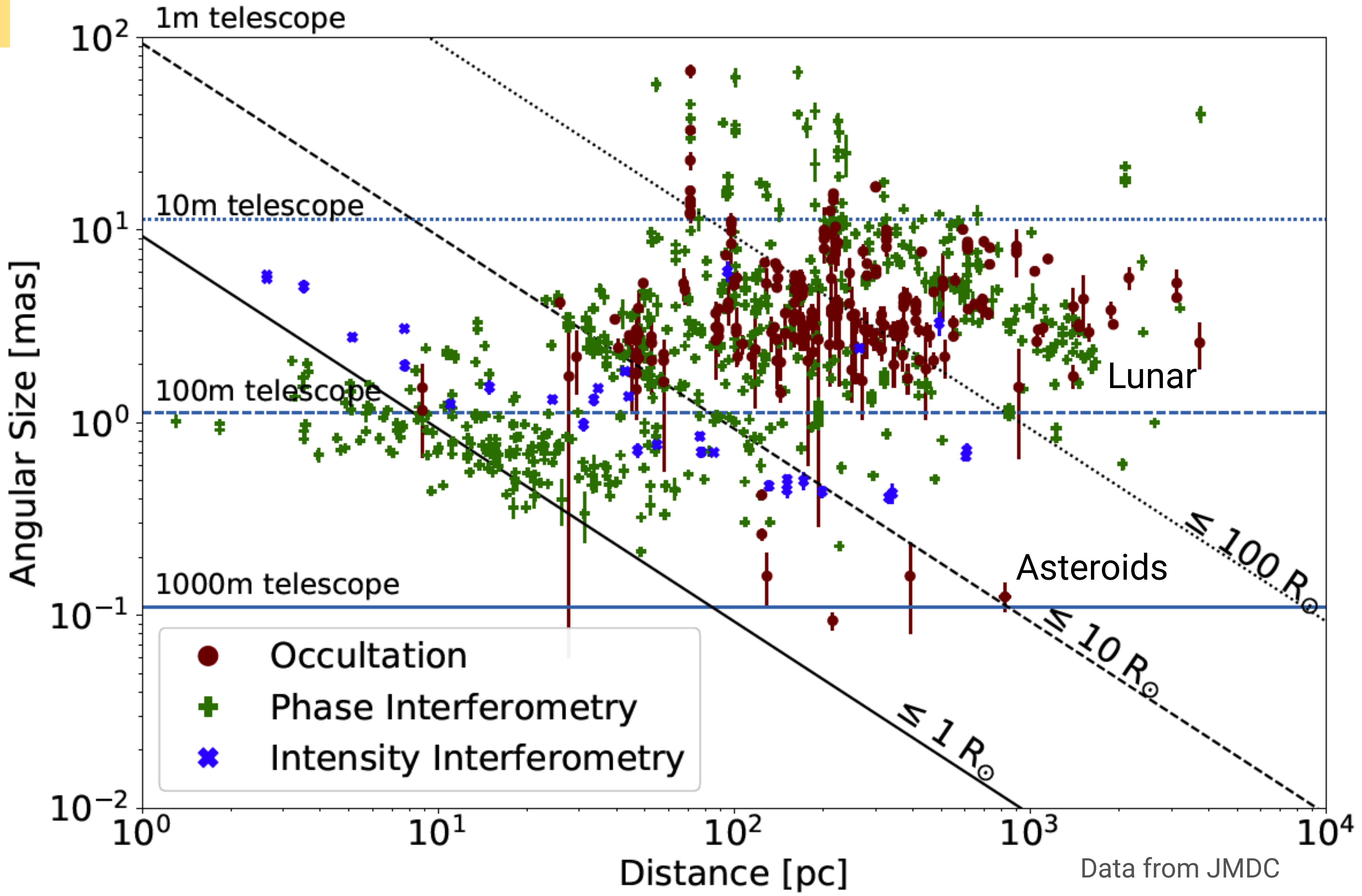

- Constrain stellar evolution models
- Also useful in determining size of transiting exo-planets

The next dimension — limb darkening

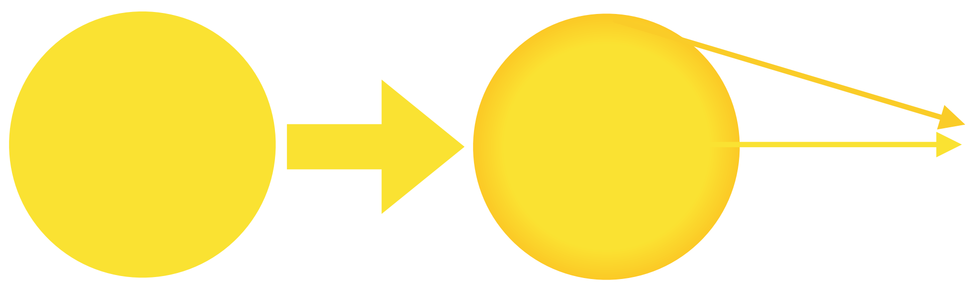

The longer the baselines, the more sensitive the observation… the more:

- **accurately** constrain stellar evolution models in a model independent way
- for <5% error can **accurately** determine size of transiting exo-planets

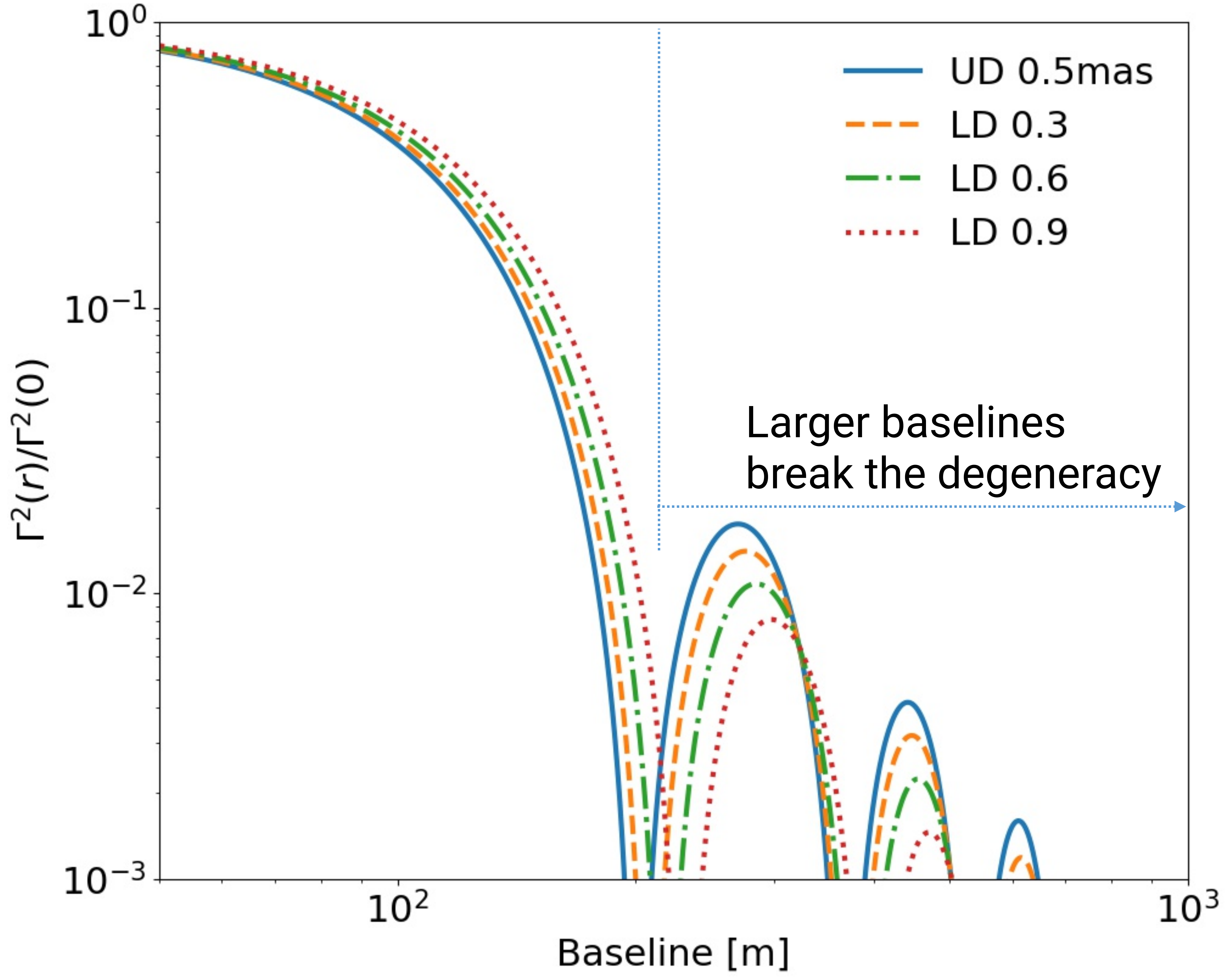

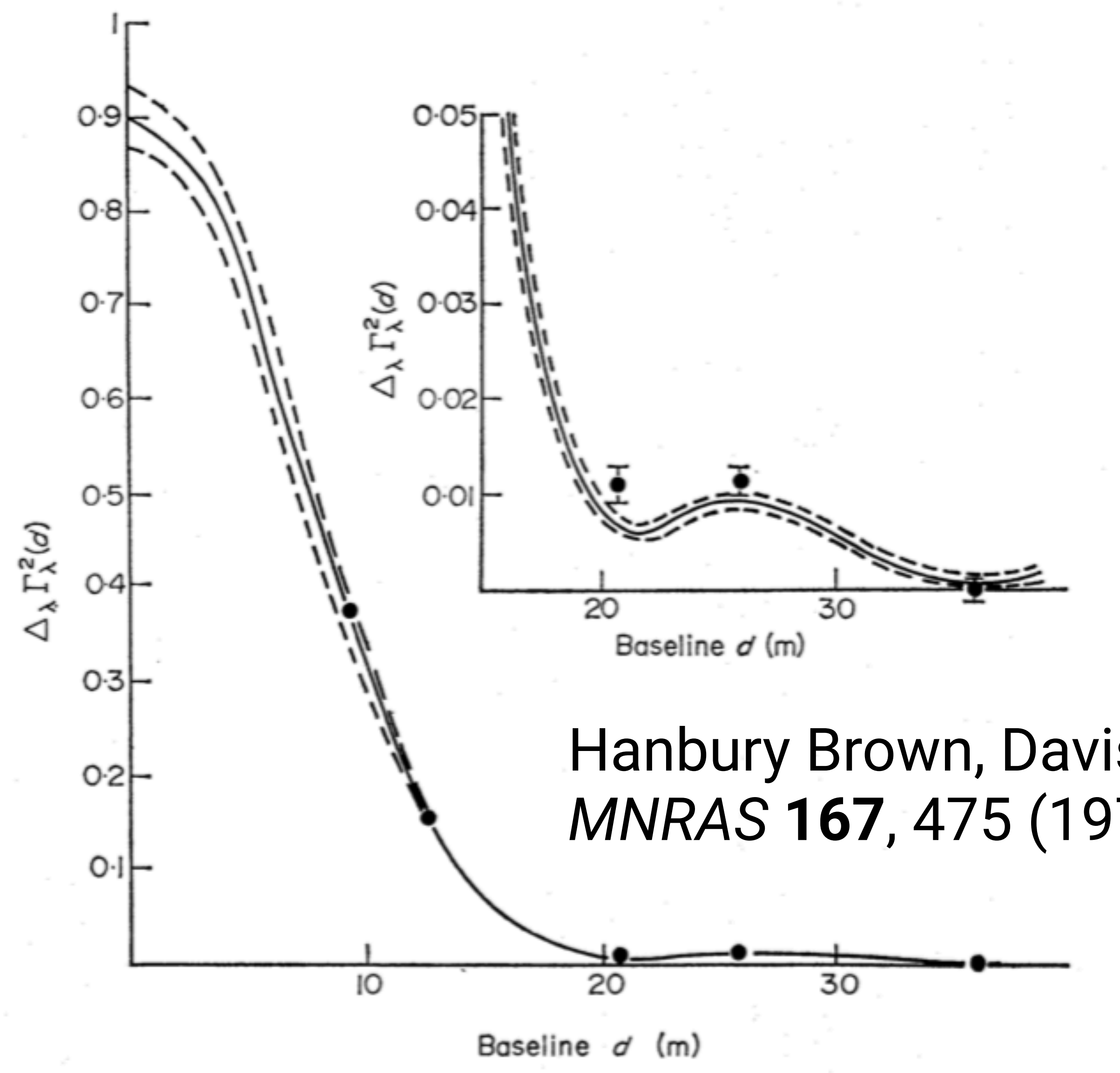

Hanbury Brown, Davis Lake & Thompson
MNRAS **167**, 475 (1974)

Fig. 3. *The variation of correlation $\Delta_\lambda\Gamma_\lambda$ (d) with baseline d for Sirius. The points show the observed values; the full line is a theoretical curve, based on a model stellar atmosphere (T_e = 10 000K, log g = 4), with zero-baseline correlation and angular size adjusted to give the best fit to the observations. The broken lines represent the rms uncertainty in the theoretical curves.*

CENTER FOR ASTROPHYSICS
HARVARD & SMITHSONIAN

Rapidly rotating stars — distorted discs — gravitational darkening — e.g. Altair

- Be star disk formation
- winds from hot stars
- Wolf-Rayet star environments
- GRB pre-cursors
- …

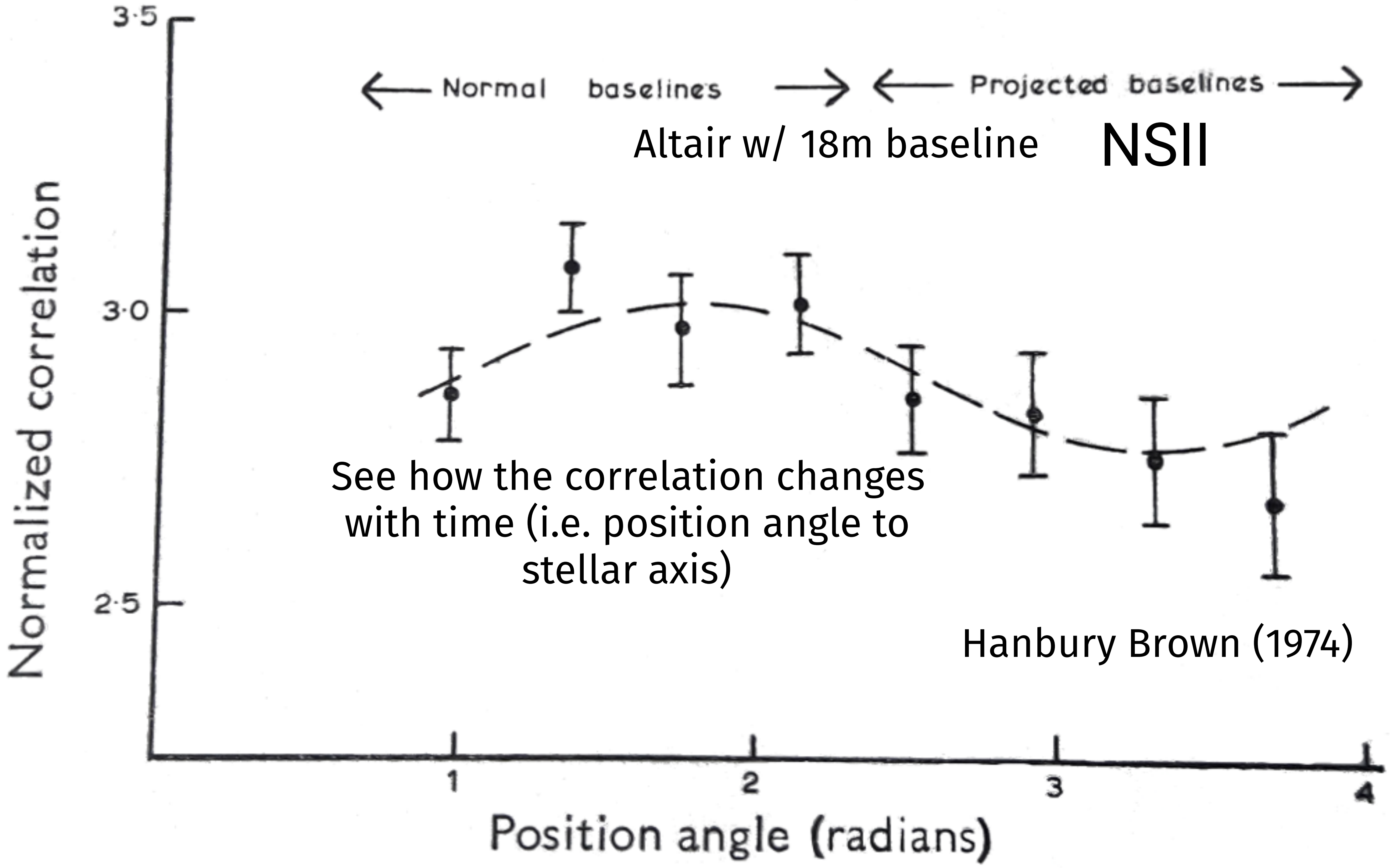

with 2 telescopes… *get an impression*

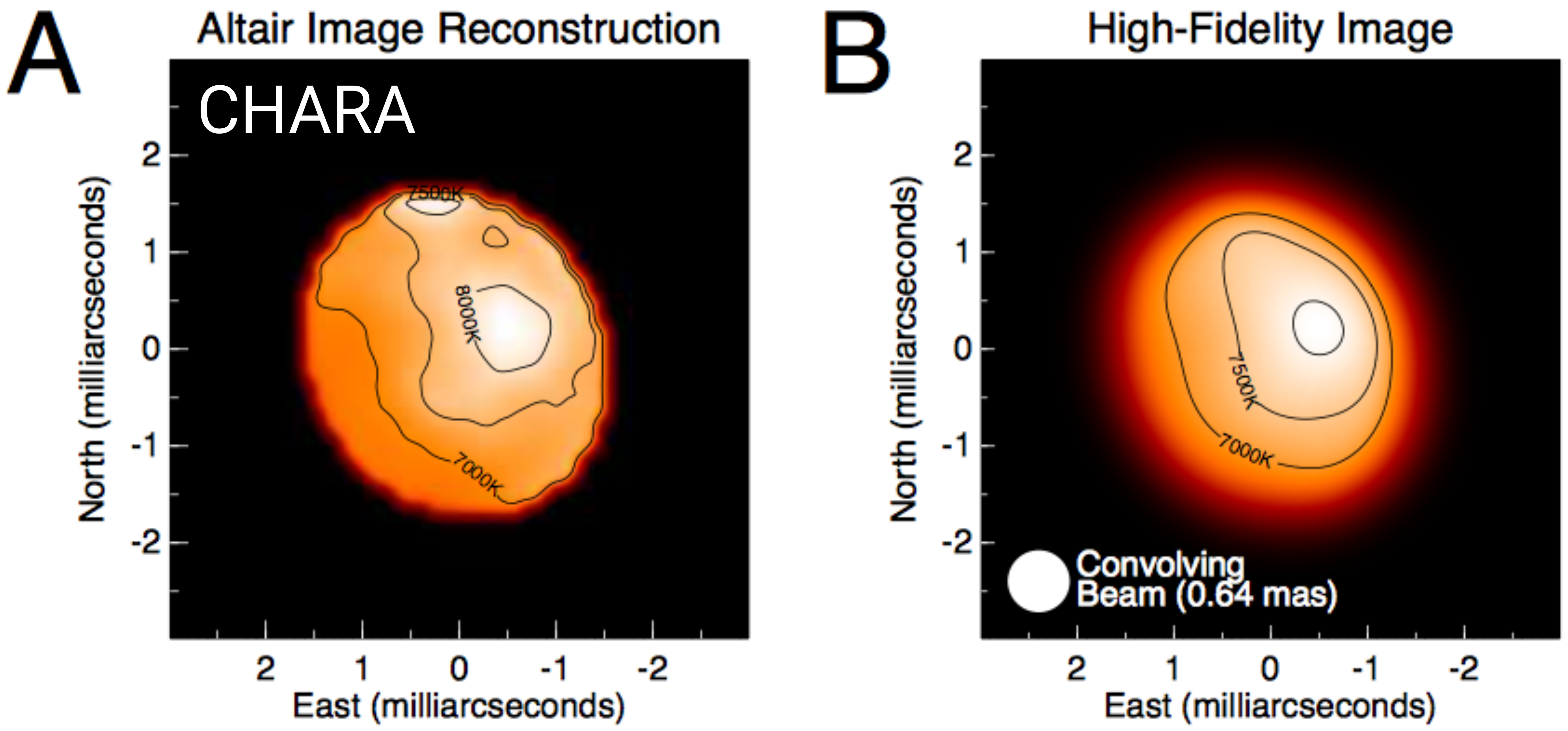

with 6 telescopes… **start to build a picture**

The difference between the CHARA observation and the theoretical model "shows stronger darkening along the equator, inconsistent with any von Zeipel-like gravity darkening prescription assuming uniform rotation."

CHARA *Science* **317**, 5836 (2007)

With more telescopes we provide the data to fit a model to, rather than vice versa

CENTER FOR ASTROPHYSICS
HARVARD & SMITHSONIAN

Binary systems & star spots & accretion zones …

Remember, these are dynamic systems.

A time averaged correlation provides some information,
a time sequence or series of images provides more

So requirements are:

- Many baselines of >100m
- Many baselines measuring simultaneously for shorter observation times

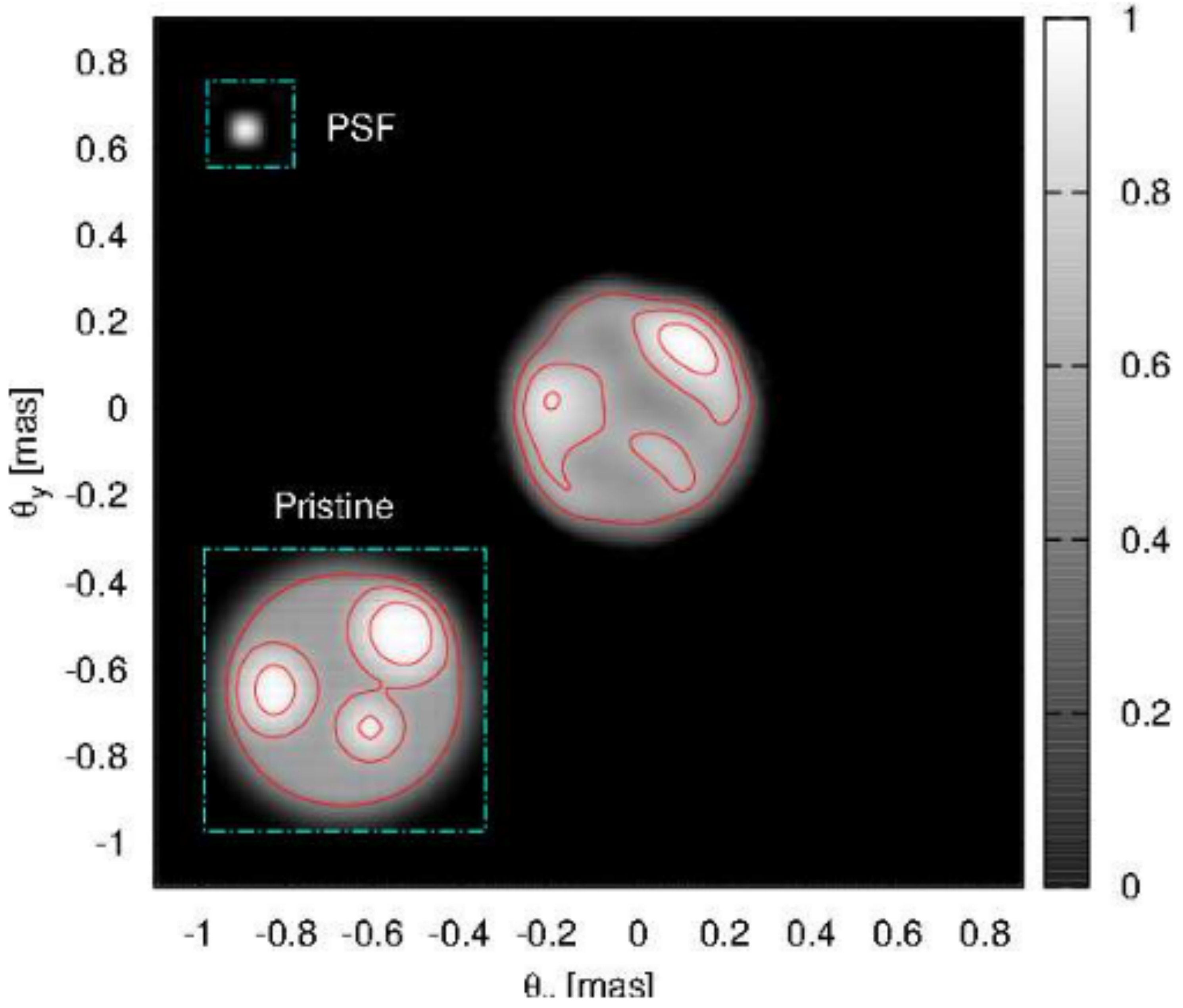

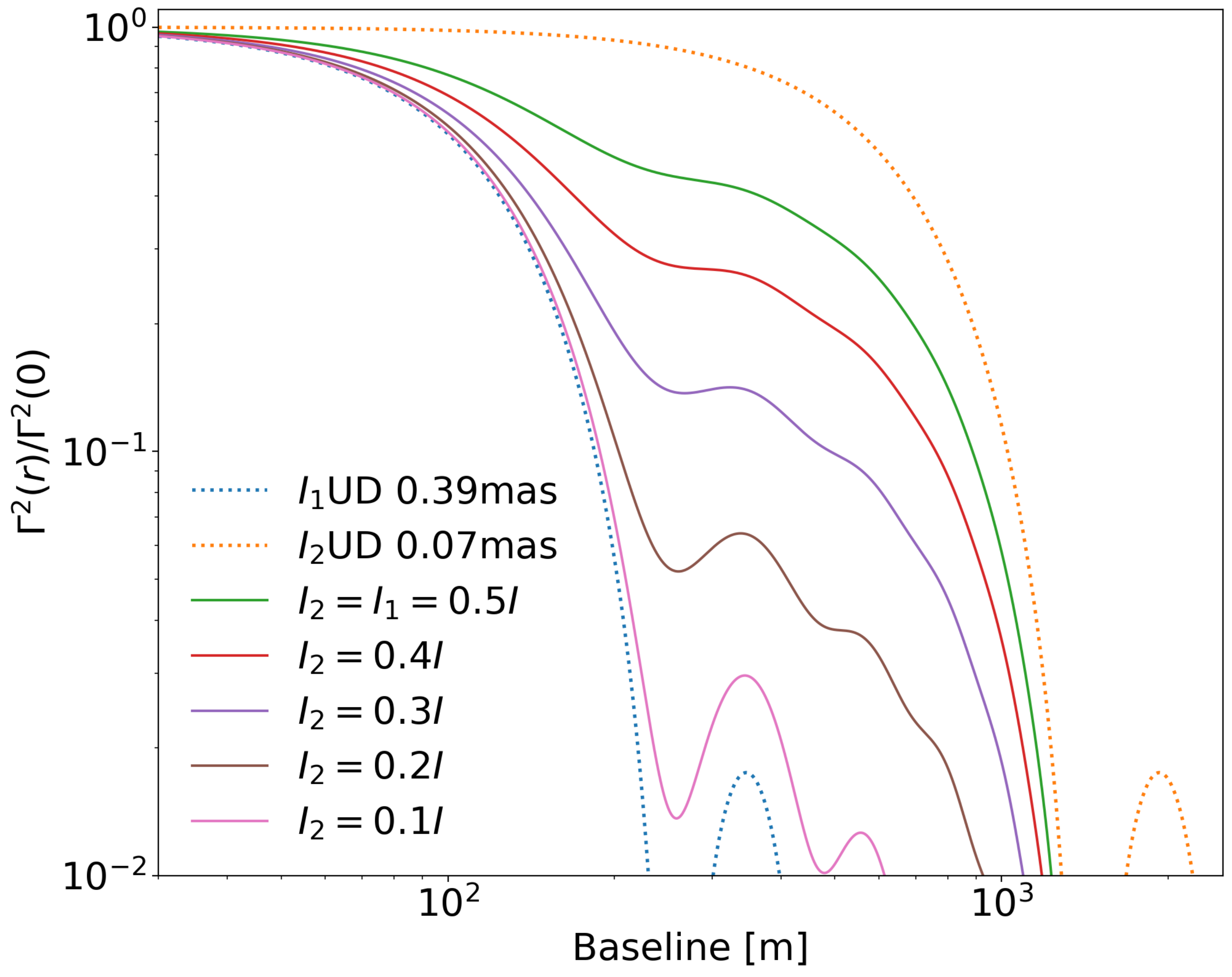

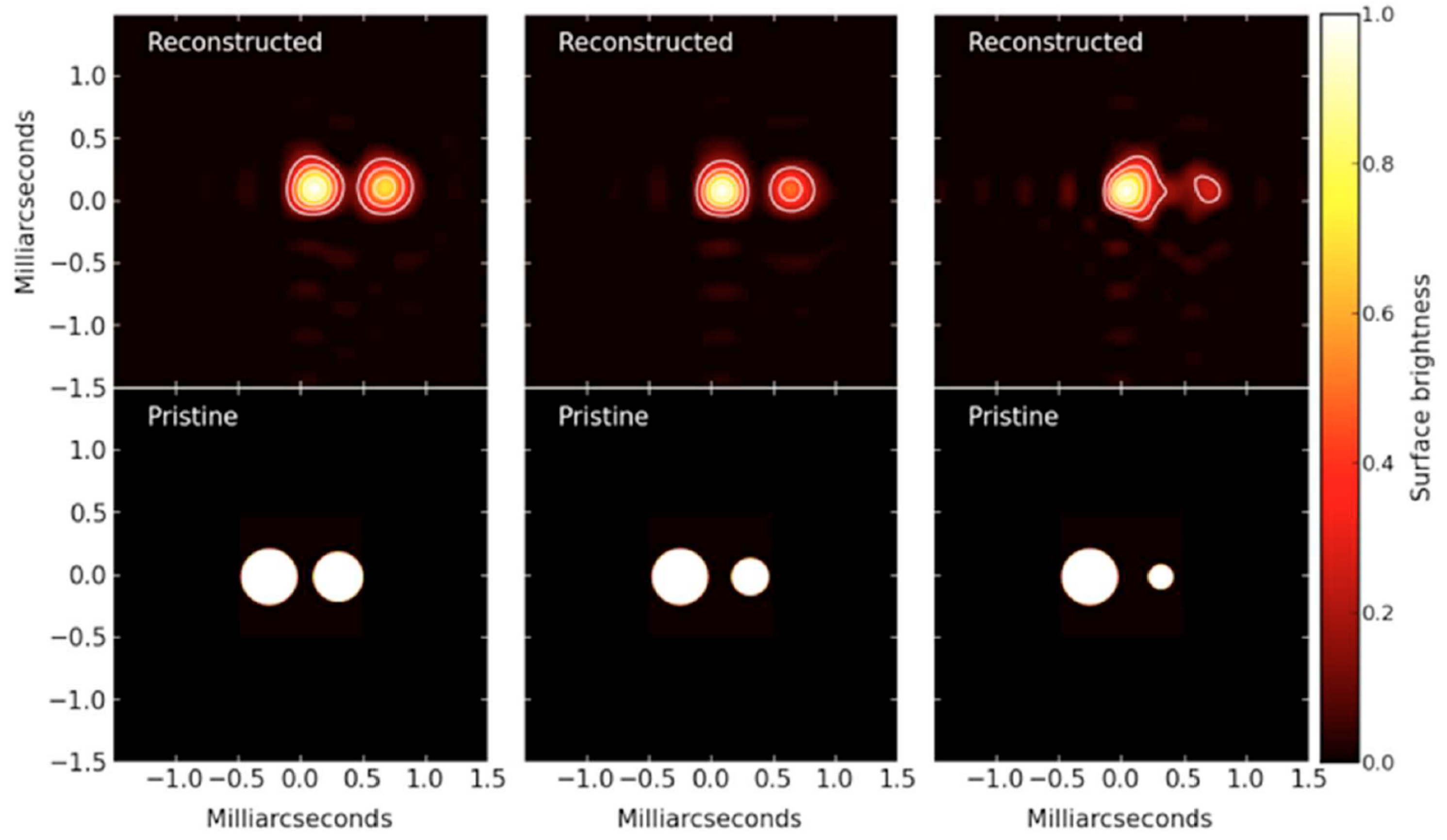

Figure 5: Reconstructed images of binary stars (with varying diameter of the secondary) from simulated CTA observations. These simulations were for the array layout B (Figure 2), for sources assumed to have visual magnitude $m_V = 3$, and effective temperature T_{eff} = 7000 K. The assumed pristine images are shown below while the corresponding (u, v)−plane coverage is in Figure 6.

APh **43**, 331 (2013).

CENTER FOR ASTROPHYSICS
HARVARD & SMITHSONIAN

A little present

Stellar intensity interferometery at VERITAS

- 4x 12m diameter telescopes, arranged on rectangular grid of ~100m
- Equipped VERITAS for SII observations (augmentation funded by an NSF-AST RAPID grant)
  - beginning October 2018 (2 telescopes)
  - 3 telescope observations began in February 2019
  - measures photon intensity at each telescope with continuous digitization directly to disk (correlation is offline)
- Goal: image ~30 nearby stars in U/V band
  - observe ±2 days from full moon (when gamma-ray observations not scheduled)
  - not a problem for bright (m<4) sources with suitable filters

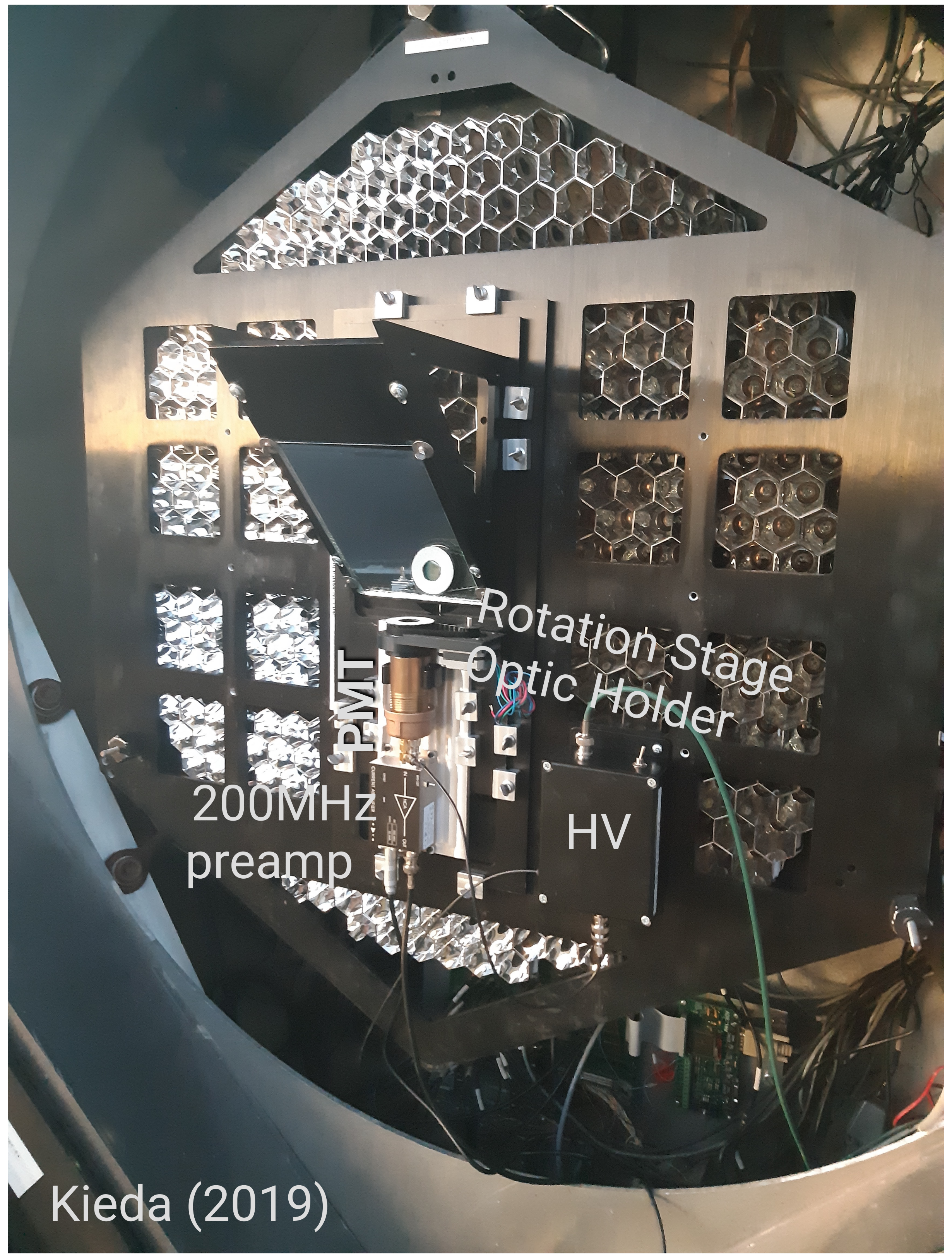

Kieda (2019)

veritas.sao.arizona.edu

CENTER FOR ASTROPHYSICS
HARVARD & SMITHSONIAN

VERITAS baselines optimal to 0.66 < θ < 1.39 mas (for zenith pointing)

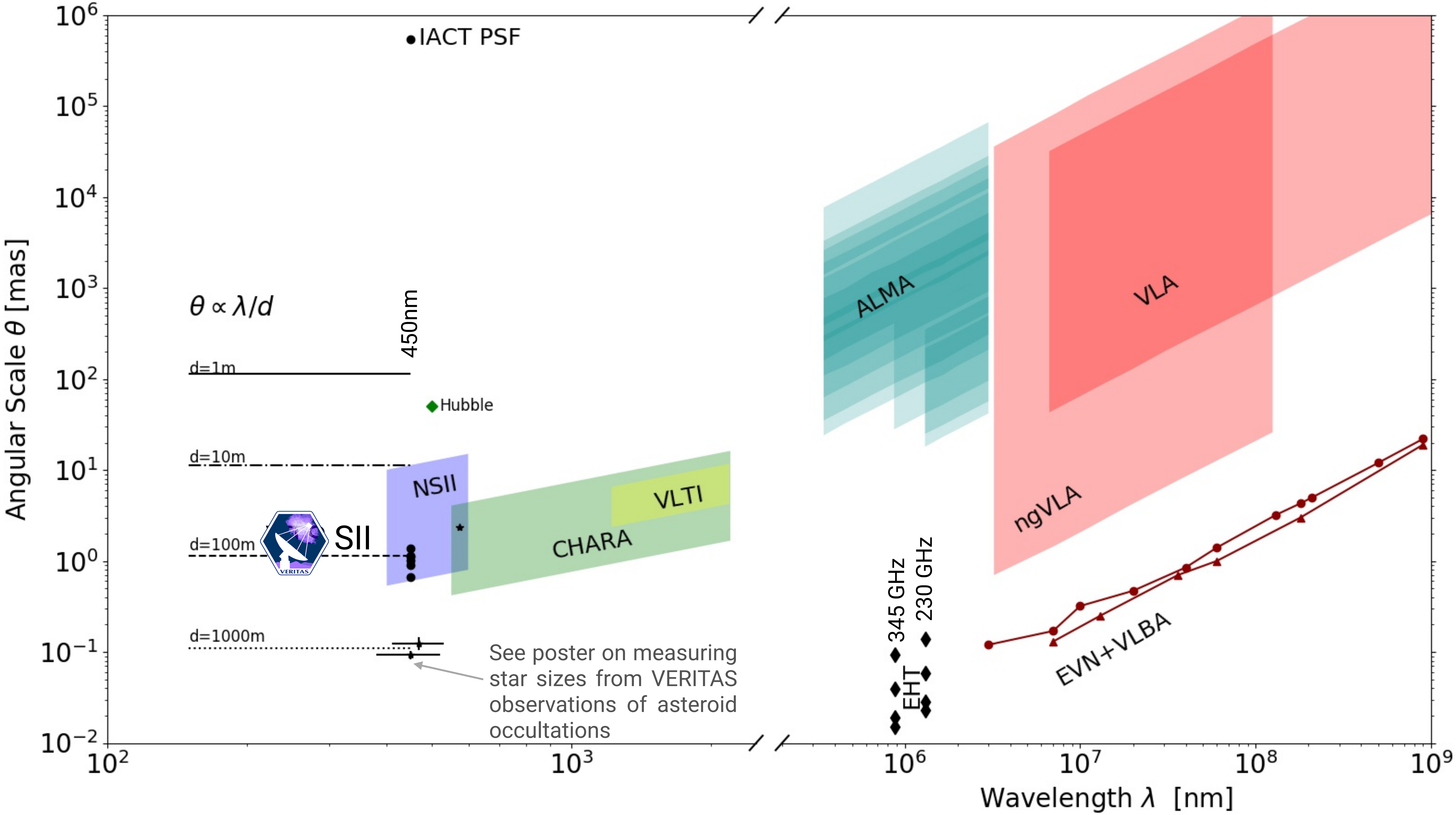

CENTER FOR ASTROPHYSICS
HARVARD & SMITHSONIAN

First Observations/ Results

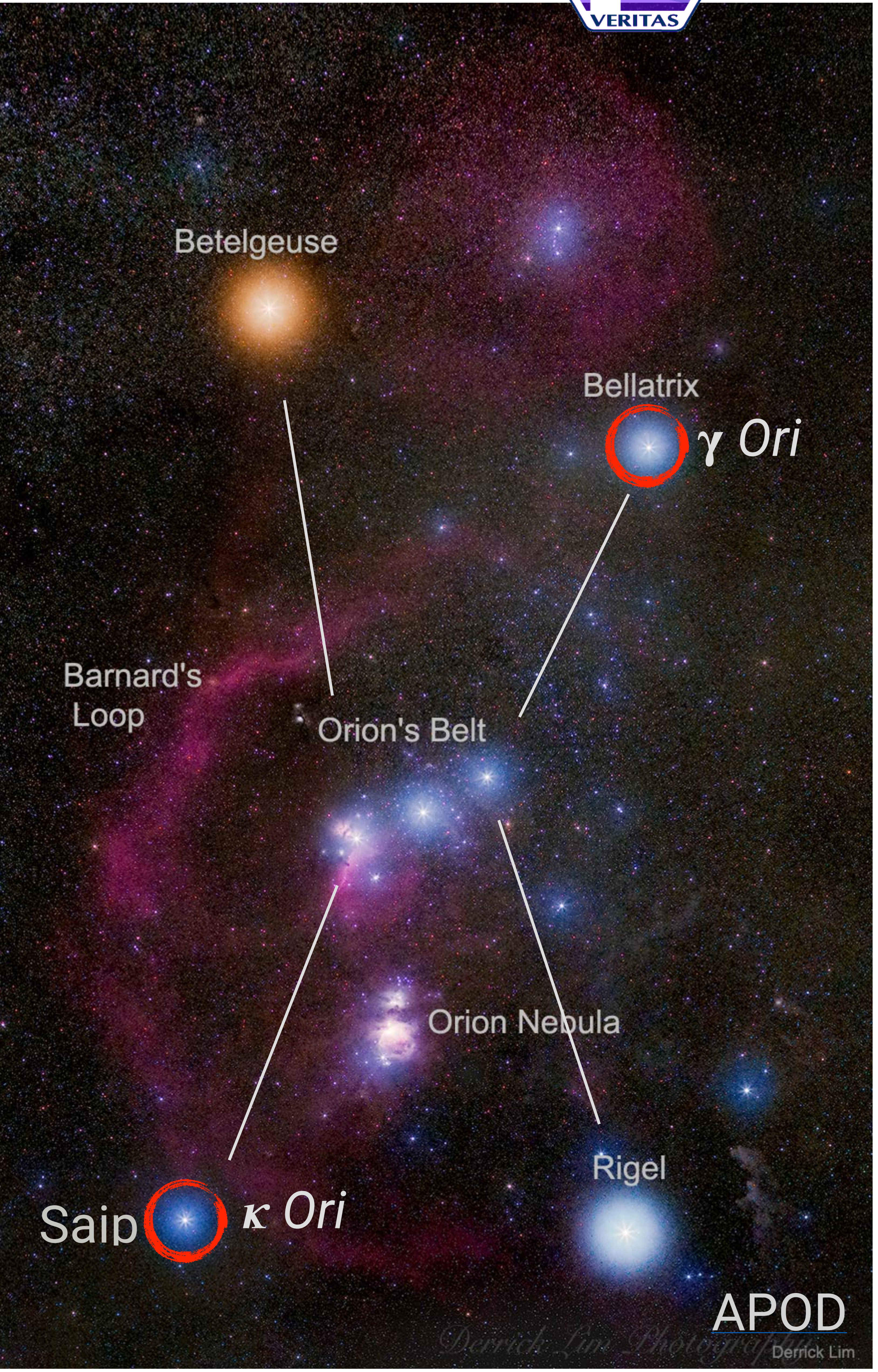

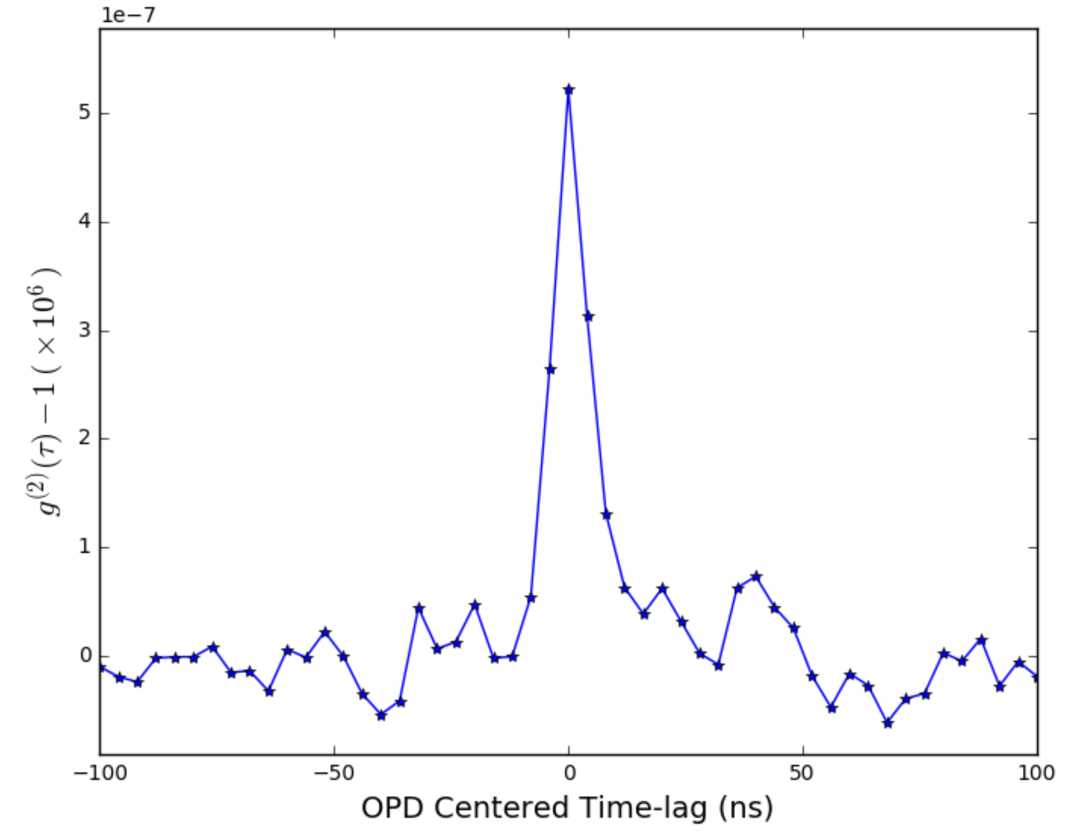

- Data taken in 20m ‘runs’
- Streamed to disk (@250MS/s)
- Correlated offline next day
  - next step, perform higher order correlations with more telescopes (phase recovery).

	T_{obs} [h]	θ_{meas} [mas]	cf θ_{UD} [mas]
γ Ori	4.74	0.68 ± 0.06	0.701 ± 0.005
κ Ori	5.13	0.48 ± 0.06	0.44 ± 0.03

Richichi et al (2005)

2 telescope results

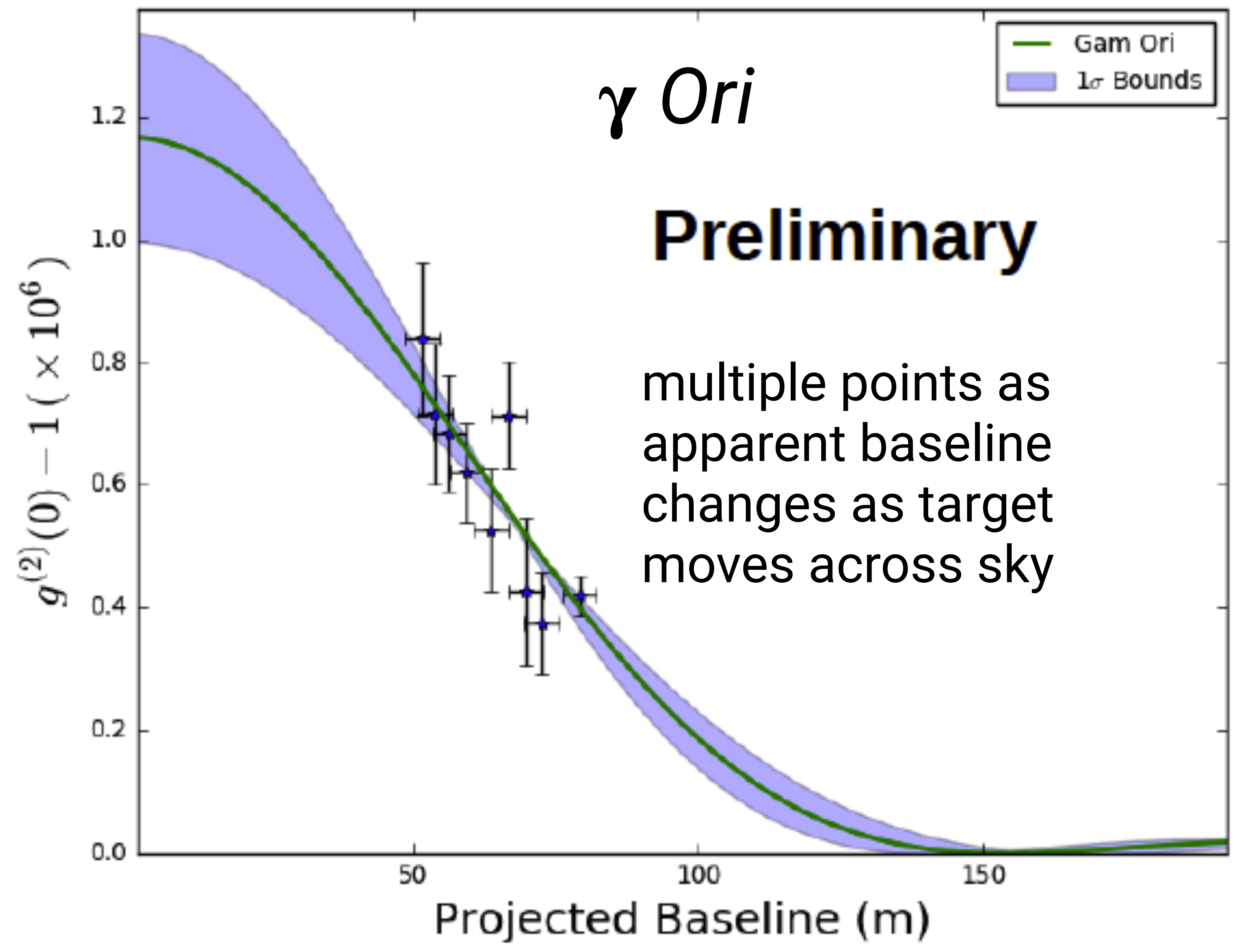

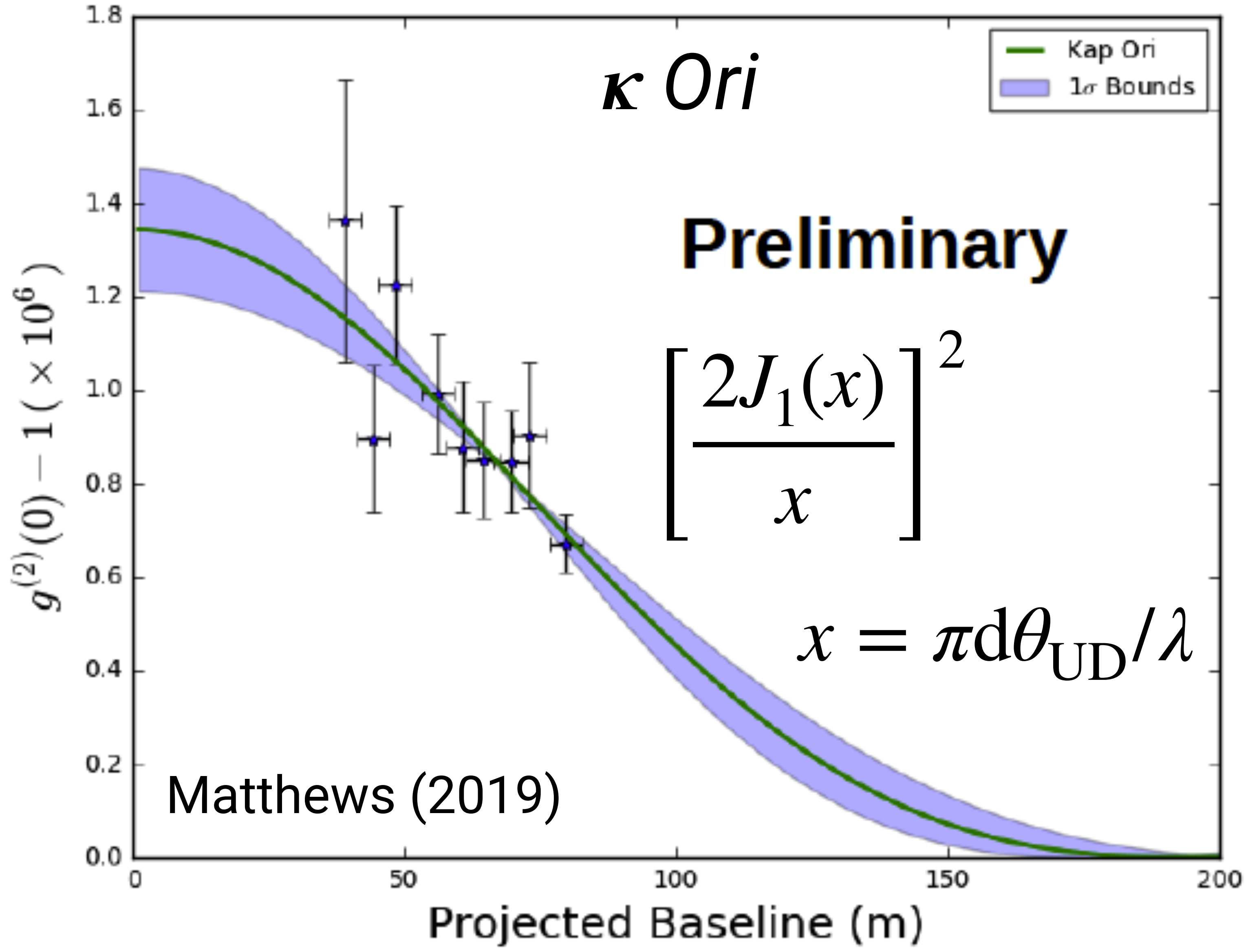

CENTER FOR ASTROPHYSICS HARVARD & SMITHSONIAN

A big future...

$$N_{pairs} = \frac{N_{tel}(N_{tel} - 1)}{2}$$

# telescopes	2	5	15	25	50	100
# baselines	1	10	105	300	1225	4950

With so many available baselines **model independent** imaging becomes a realistic possibility

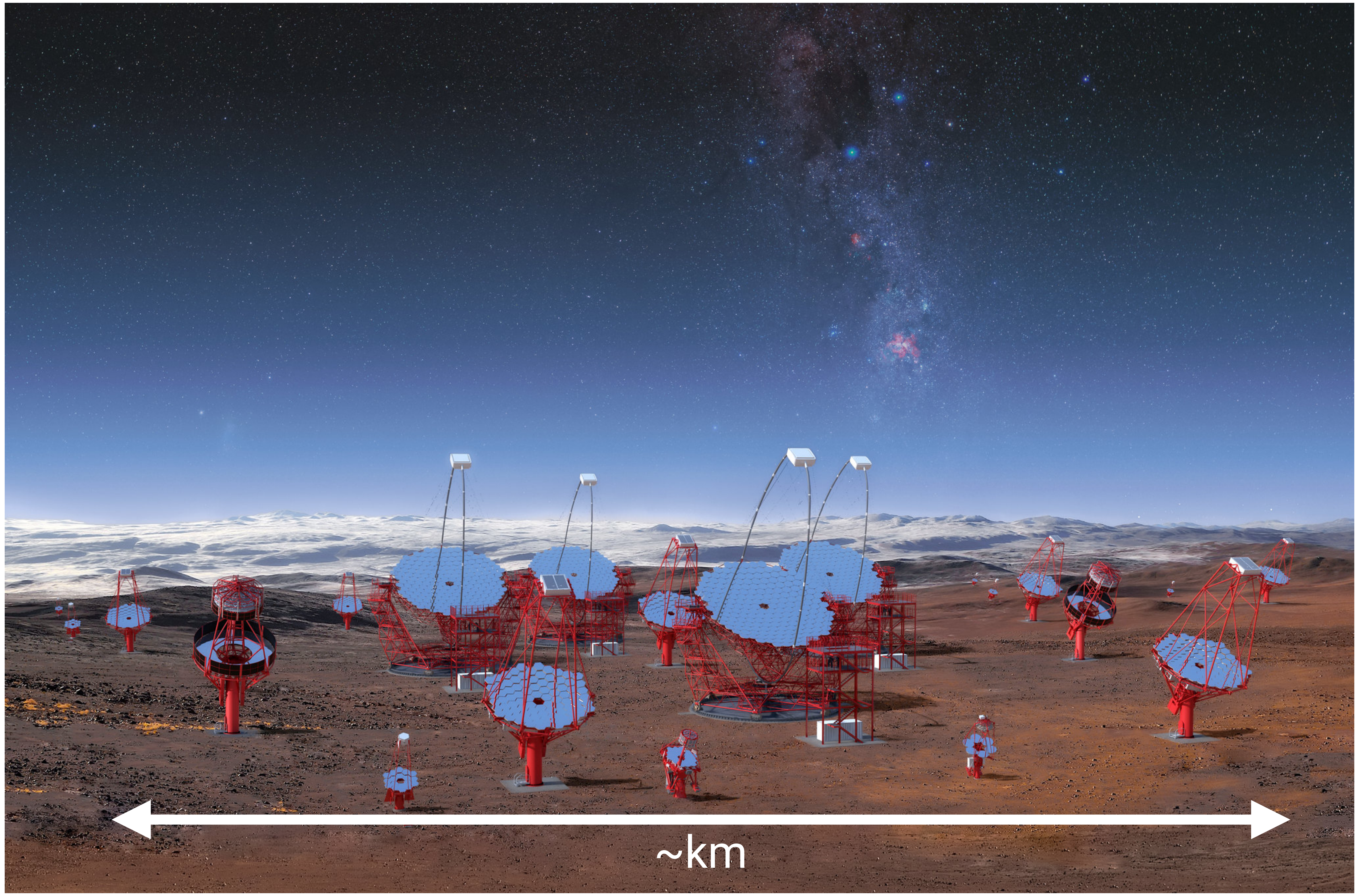

CTA brings resolving power to the next level

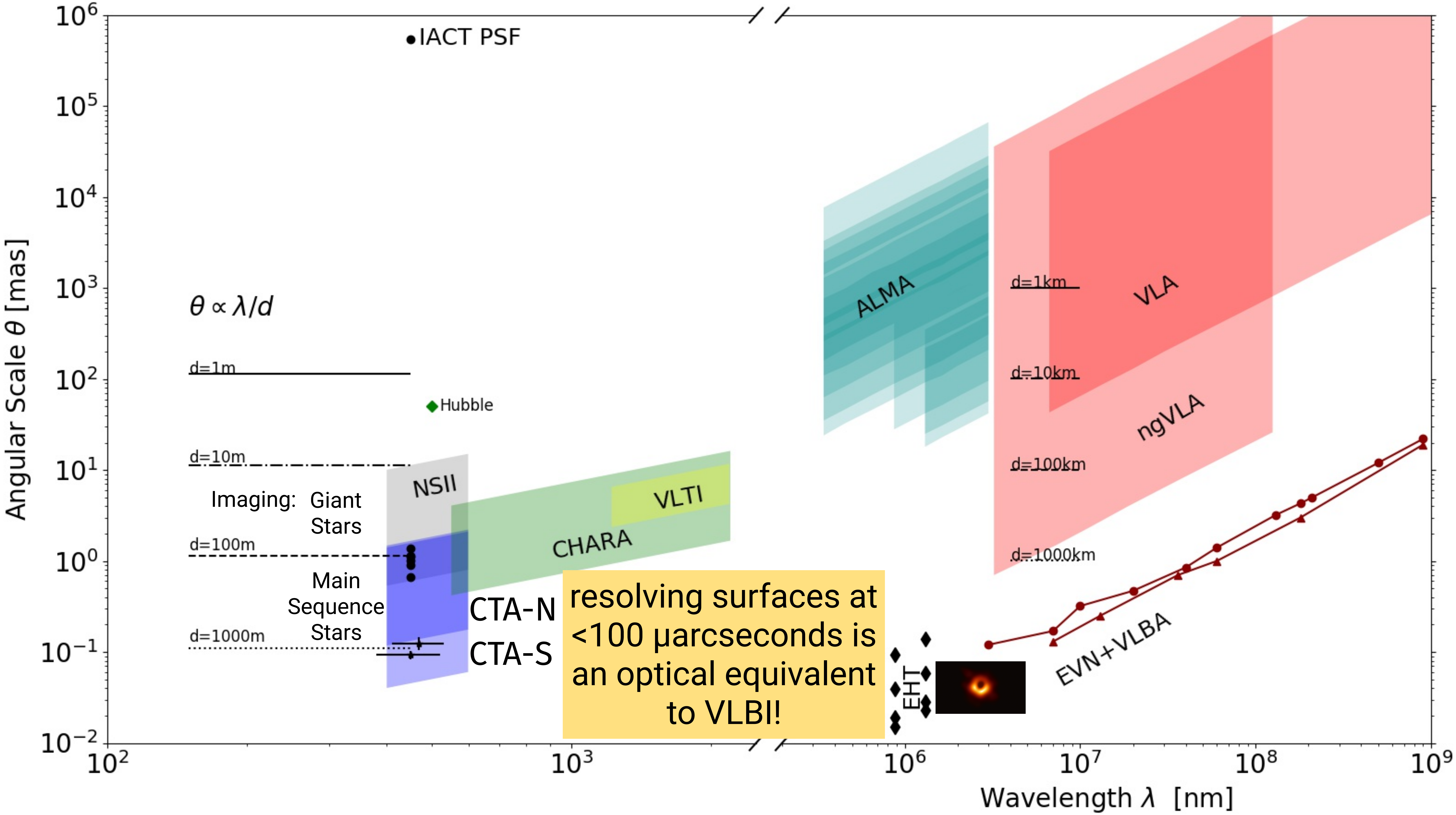

CENTER FOR ASTROPHYSICS
HARVARD & SMITHSONIAN

More than one-dimension: imaging with optical aperture synthesis

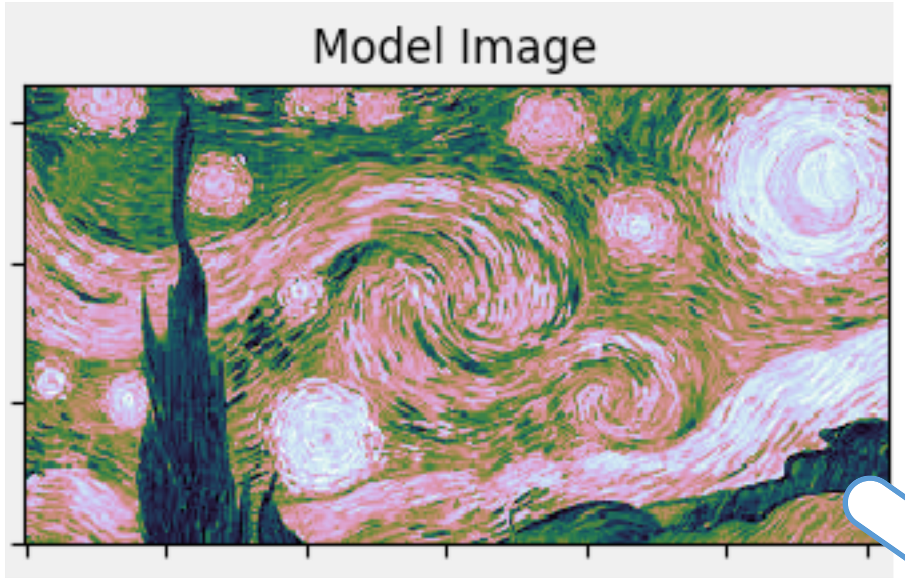

Take a few telescopes

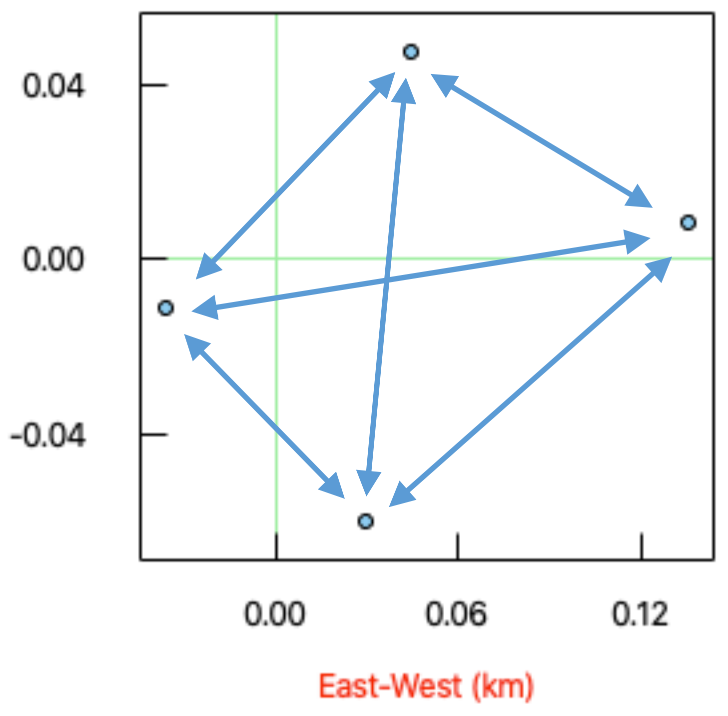

Source tracks through the sky increasing number of available baselines.

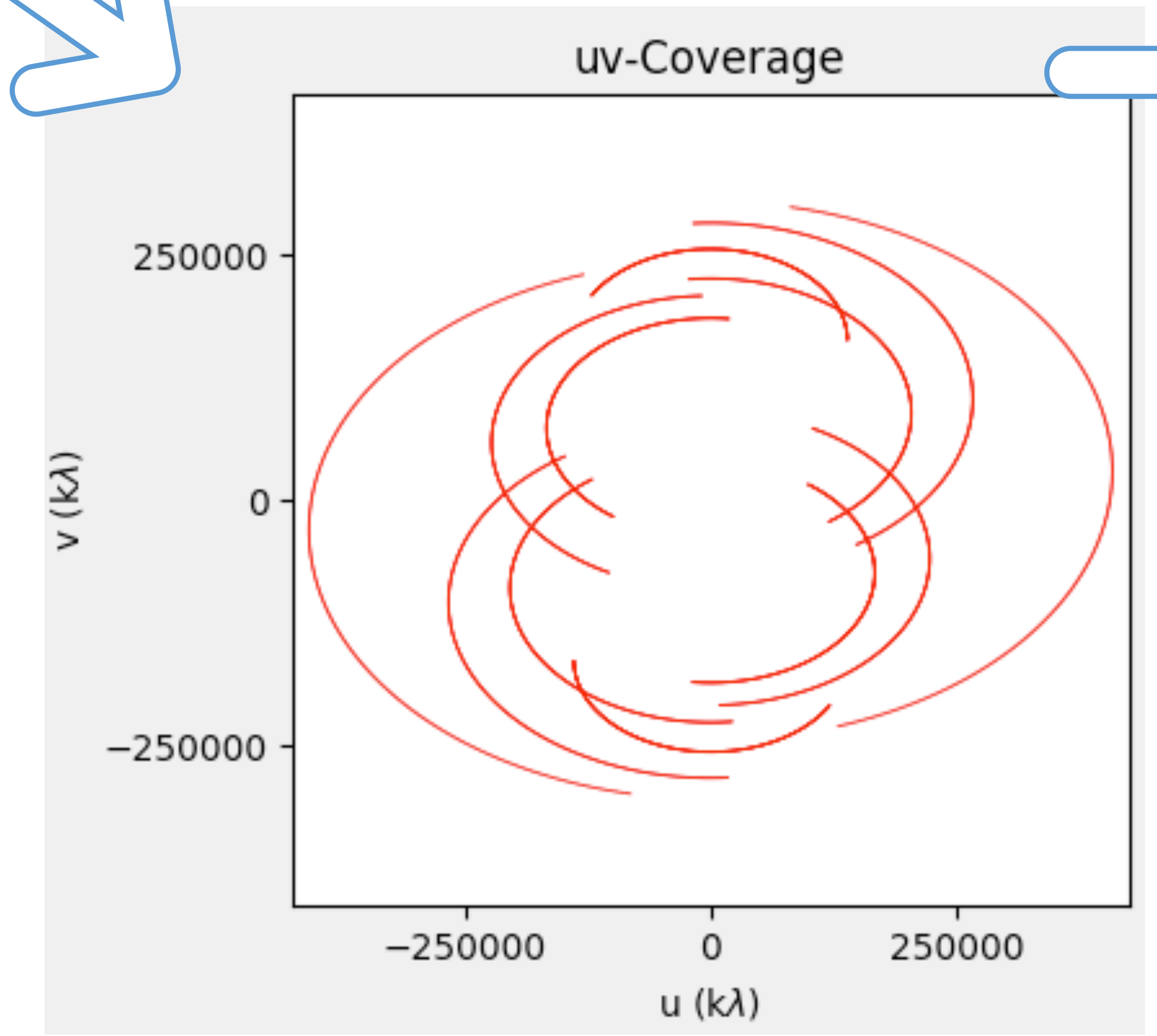

Sampling more of the Fourier spatial distribution of the observed target brightness.

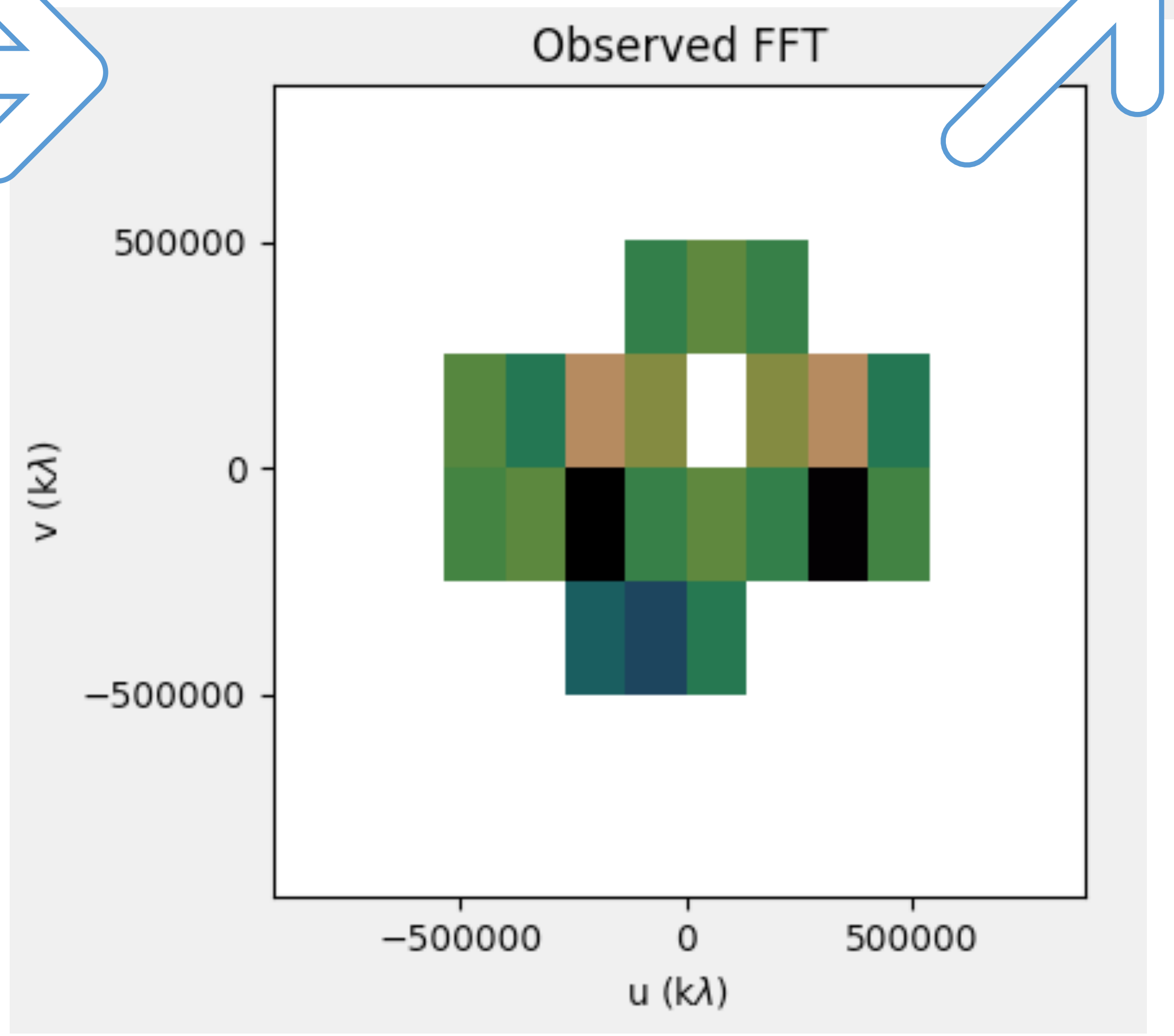

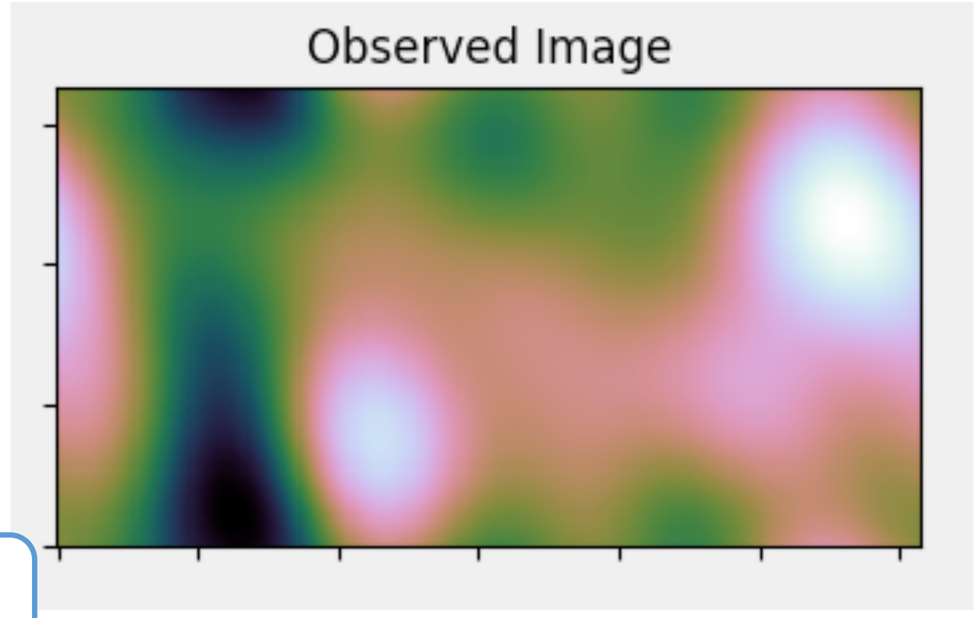

But, II measures the square of the visibility, so phase information lost.
However, there are ways to recover this.

- e.g. Cauchy-Riemann algorithm Nuñez et al. MNRAS (2012).
- e.g. three point intensity correlations Nuñez & Domiciano de Souza MNRAS (2015).

The VERITAS spacing is okay for large structure, but not for fine details

8h observation with VERITAS for a <10mas giant “solar-like” star at 20° declination

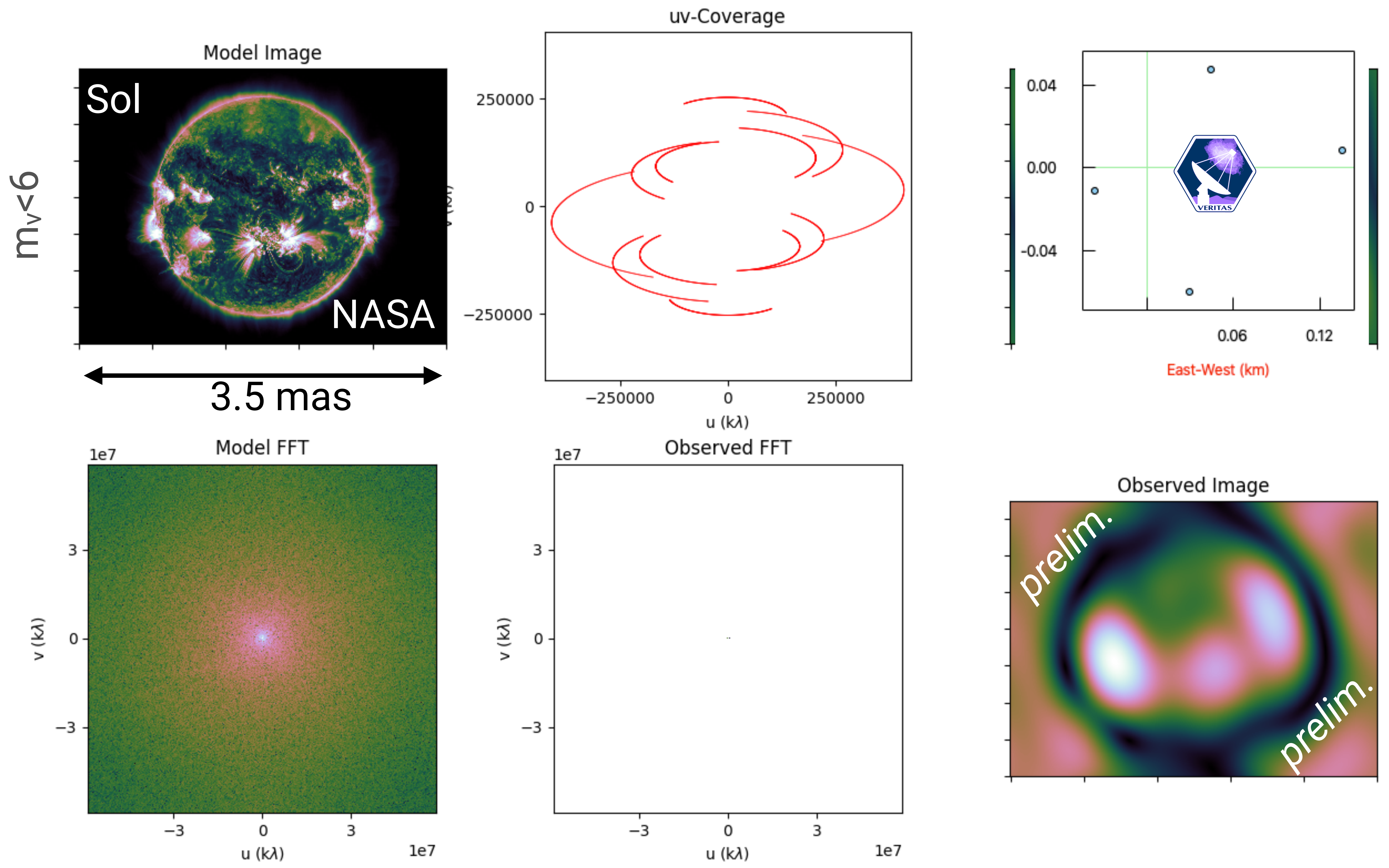

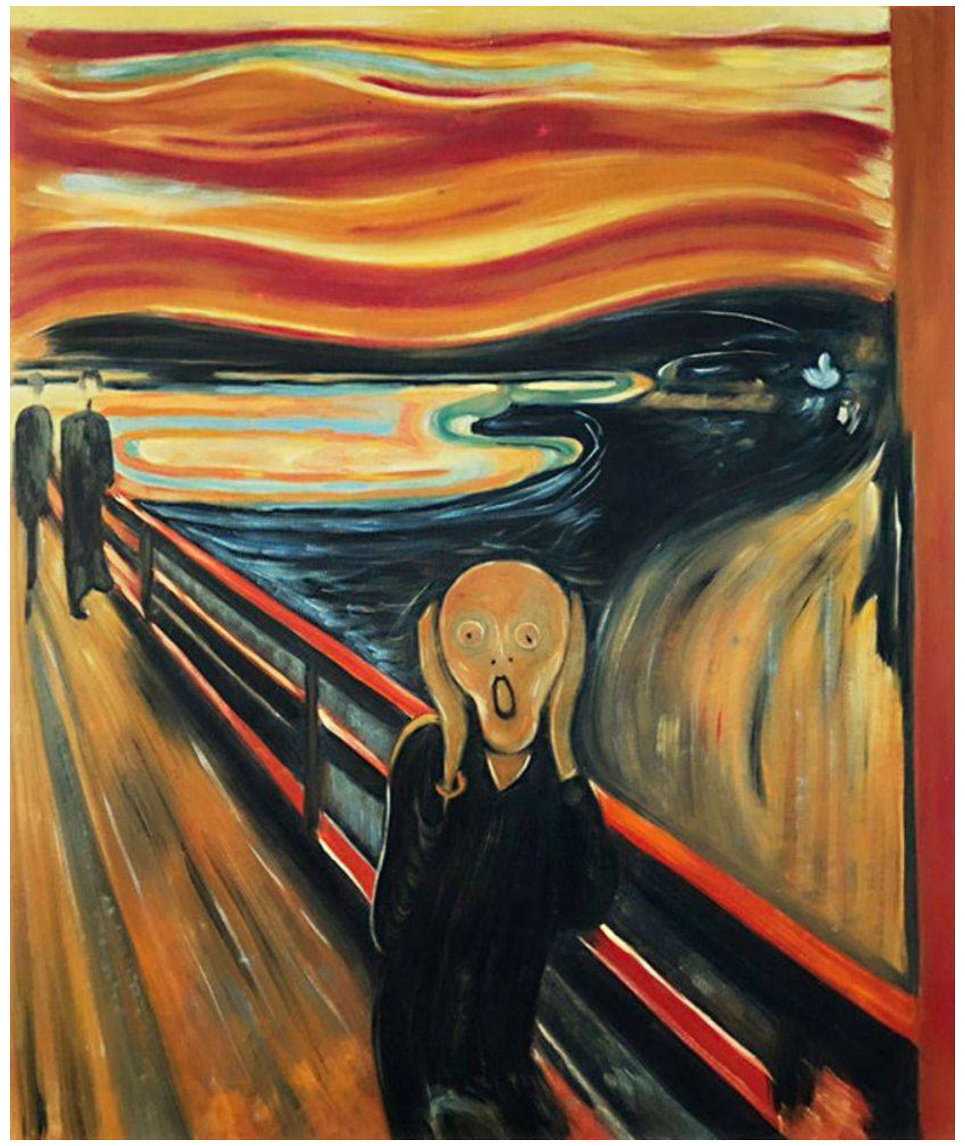

To do:

- *estimate noise*
- *phase recovery*
- **Get more telescopes**

Simulation adapted from the friendlyVRI
https://crpurcell.github.io/friendlyVRI/

*** FFT sampling effects only ***

The VERITAS spacing is okay for large structure, but not for fine details

2h observation with CTA-S SSTs for a <10mas giant “solar-like” star at -20° declination

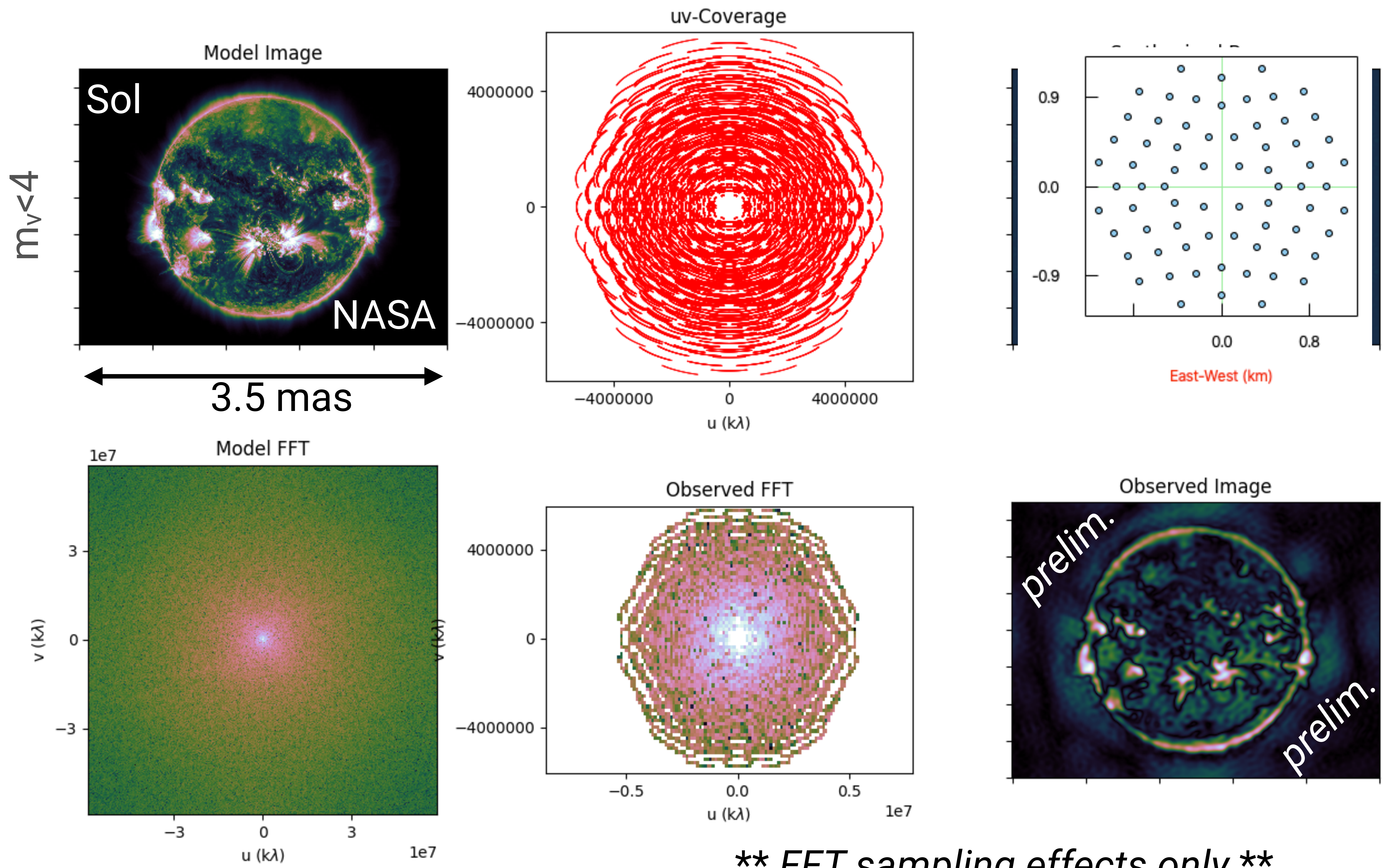

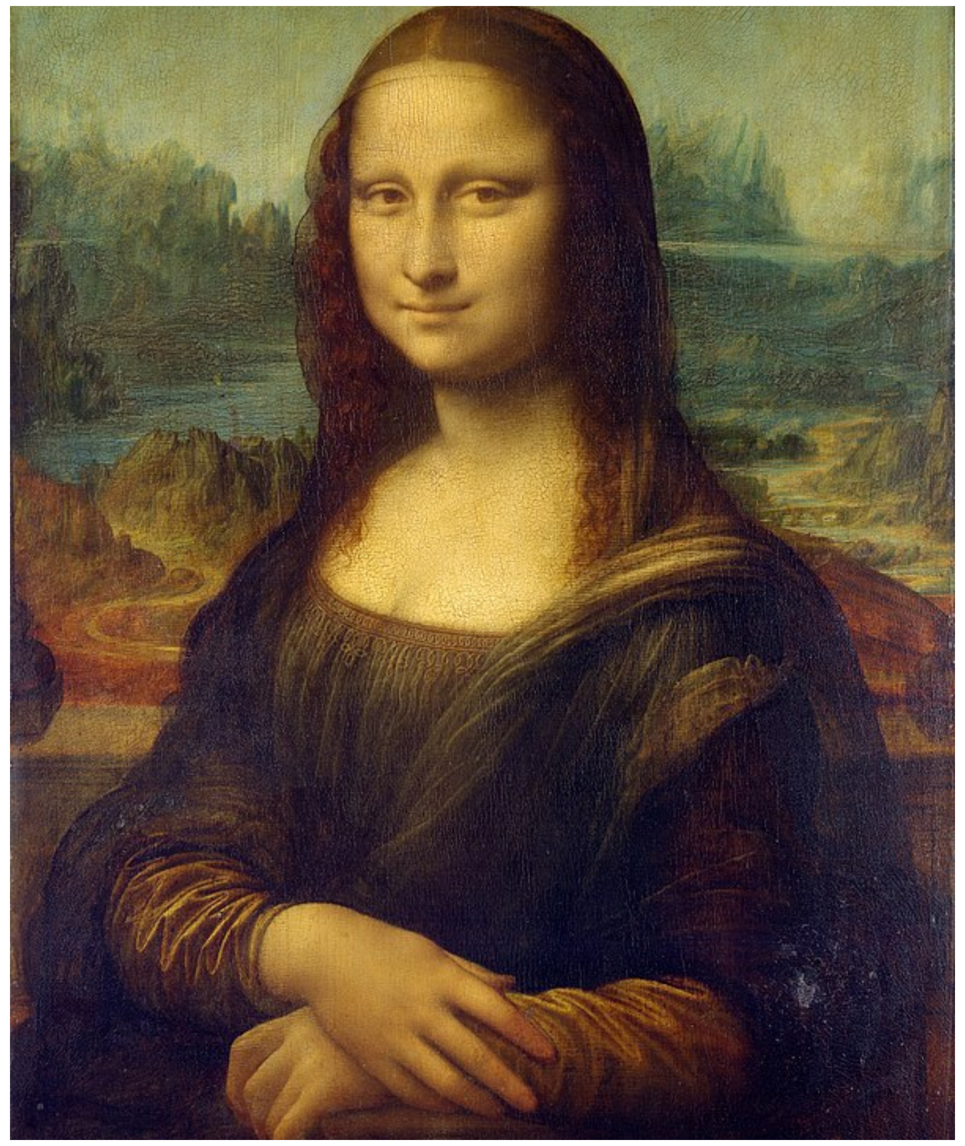

to do:

- estimate noise
- phase recovery methods
  - e.g. Cauchy-Riemann algorithm Nuñez et al. MNRAS (2012).
  - e.g. three point intensity correlations Nuñez & Domiciano de Souza MNRAS (2015).

*** FFT sampling effects only ***

Simulation adapted from the friendlyVRI
https://crpurcell.github.io/friendlyVRI/

CENTER FOR ASTROPHYSICS
HARVARD & SMITHSONIAN

8h observation with VERITAS for a <1mas “solar-like” star at 20° declination

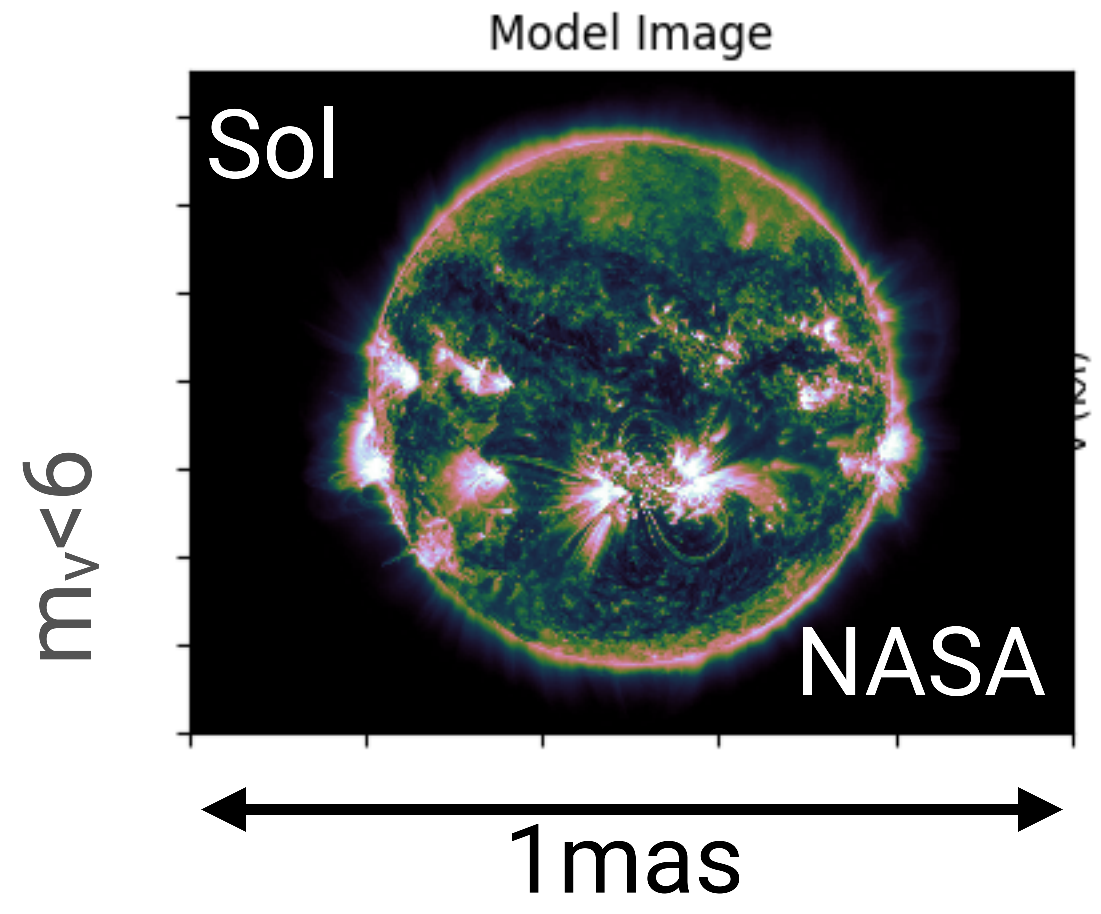

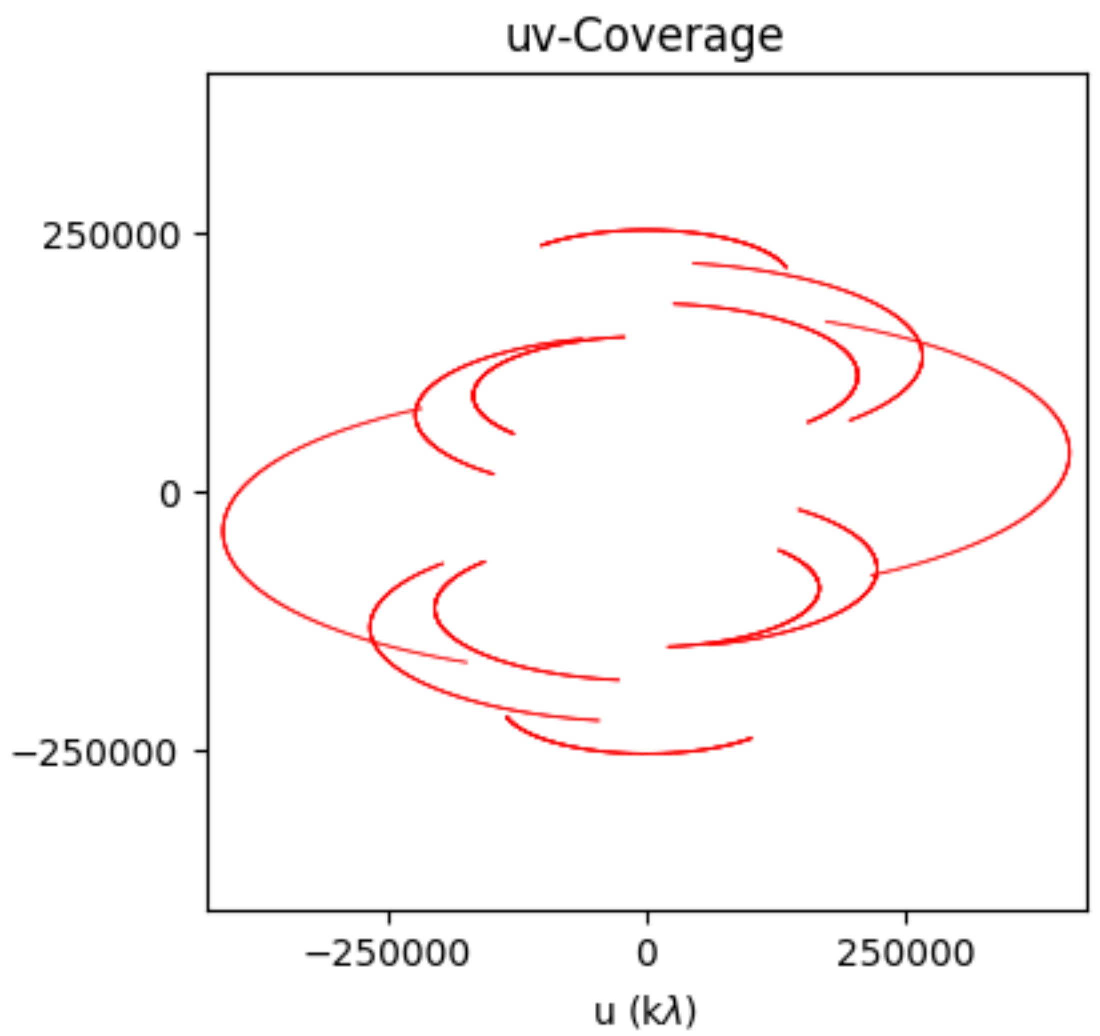

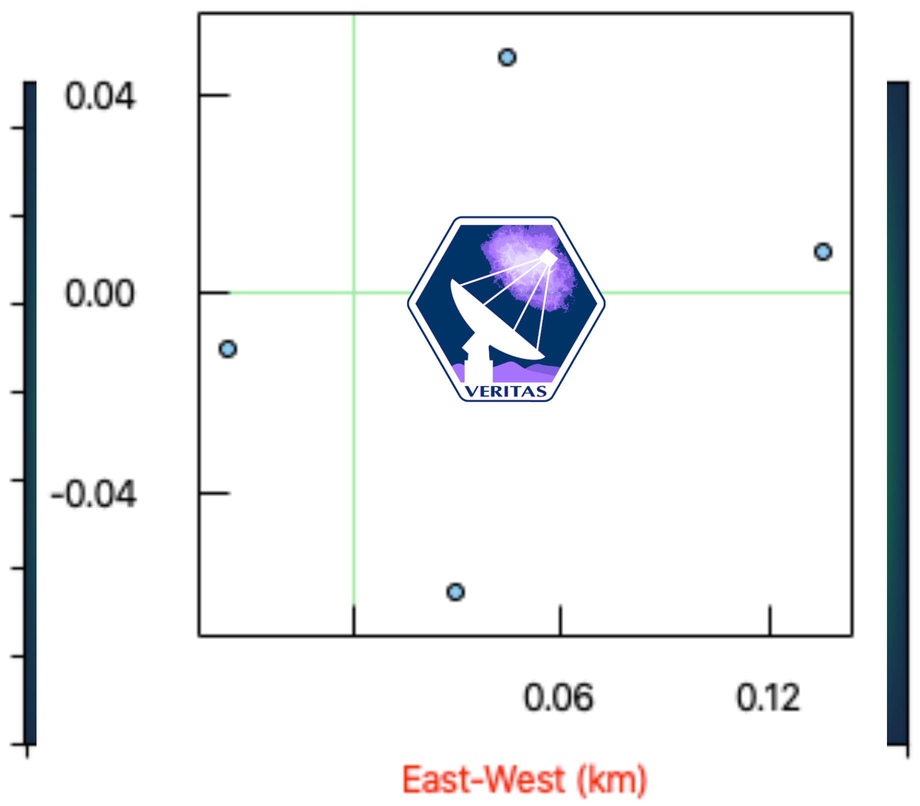

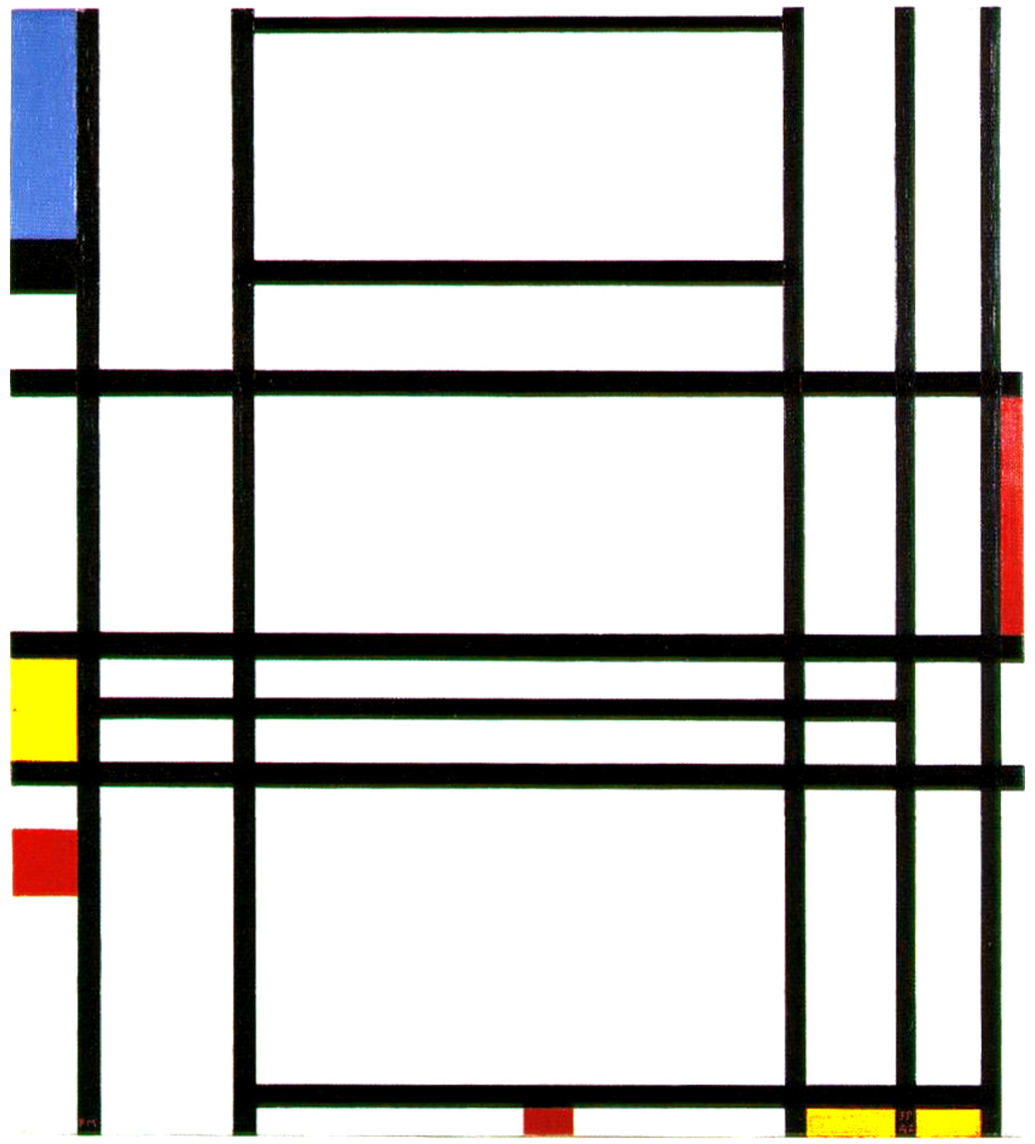

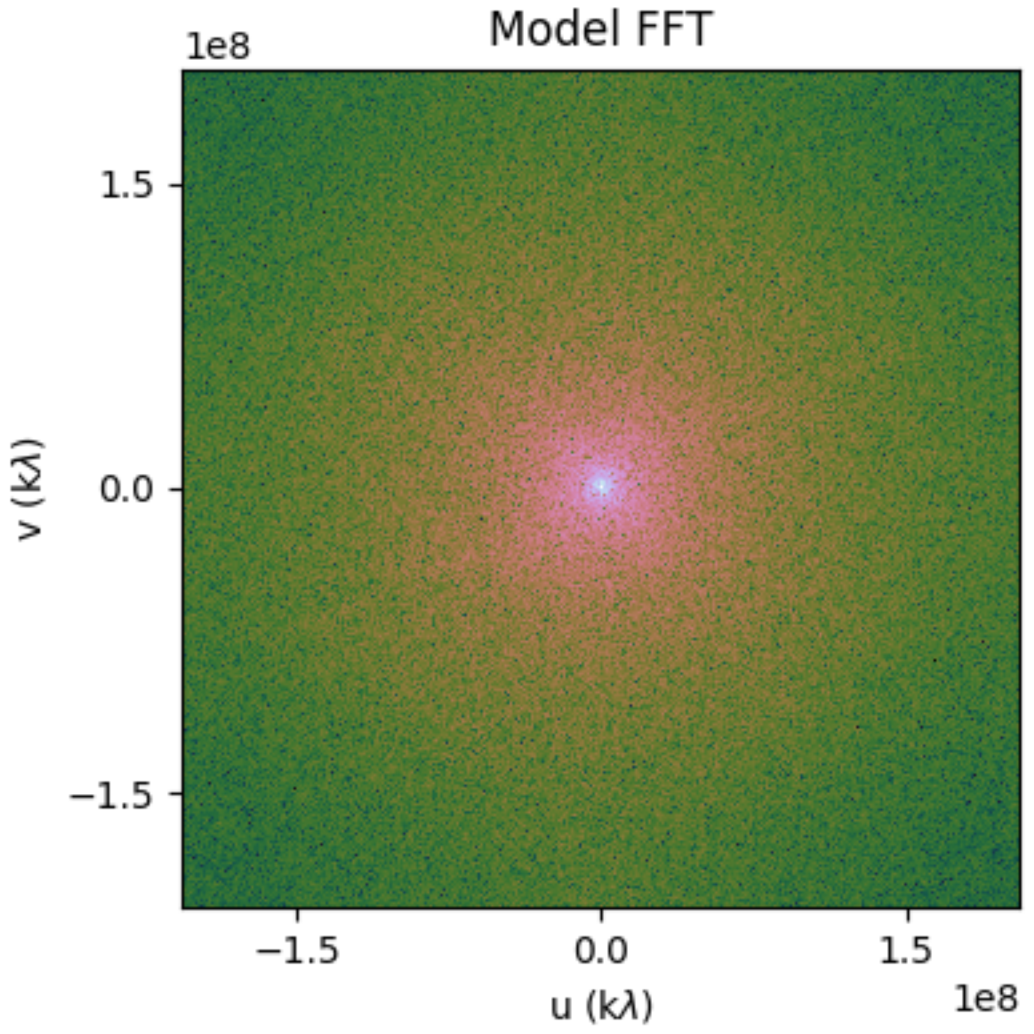

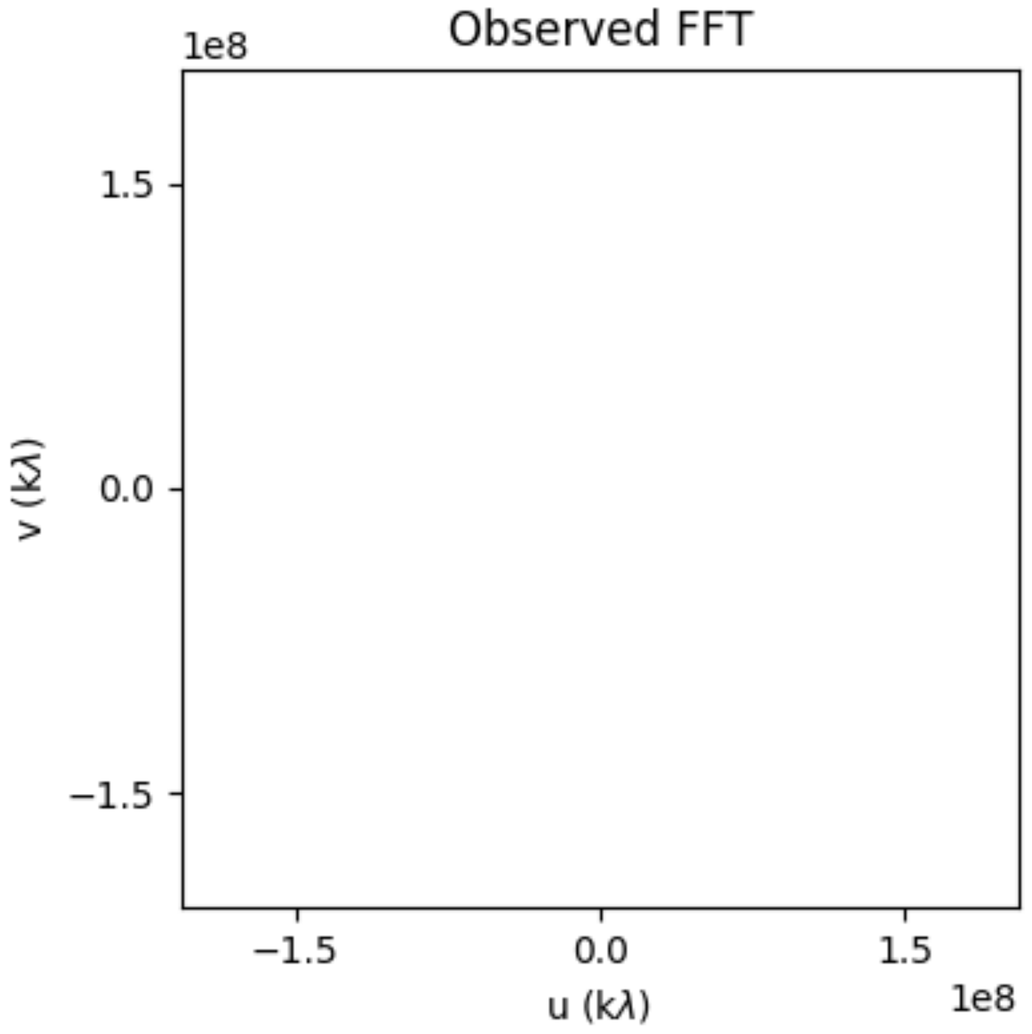

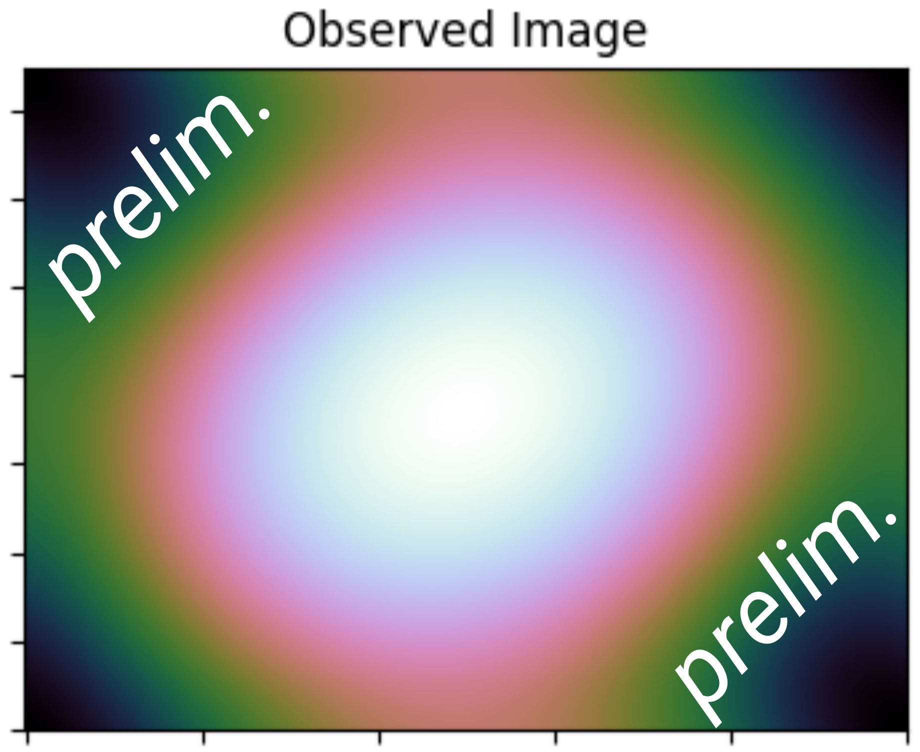

To do:

- **Get larger telescope separation**
- *estimate noise*
- *phase recovery*

Remember the interferometer is “blind” to any scale that does not have a baseline measurement

Simulation adapted from the friendlyVRI
https://crpurcell.github.io/friendlyVRI/

8h observation with CTA-S MSTs for a <1mas “solar-like” star at -20° declination

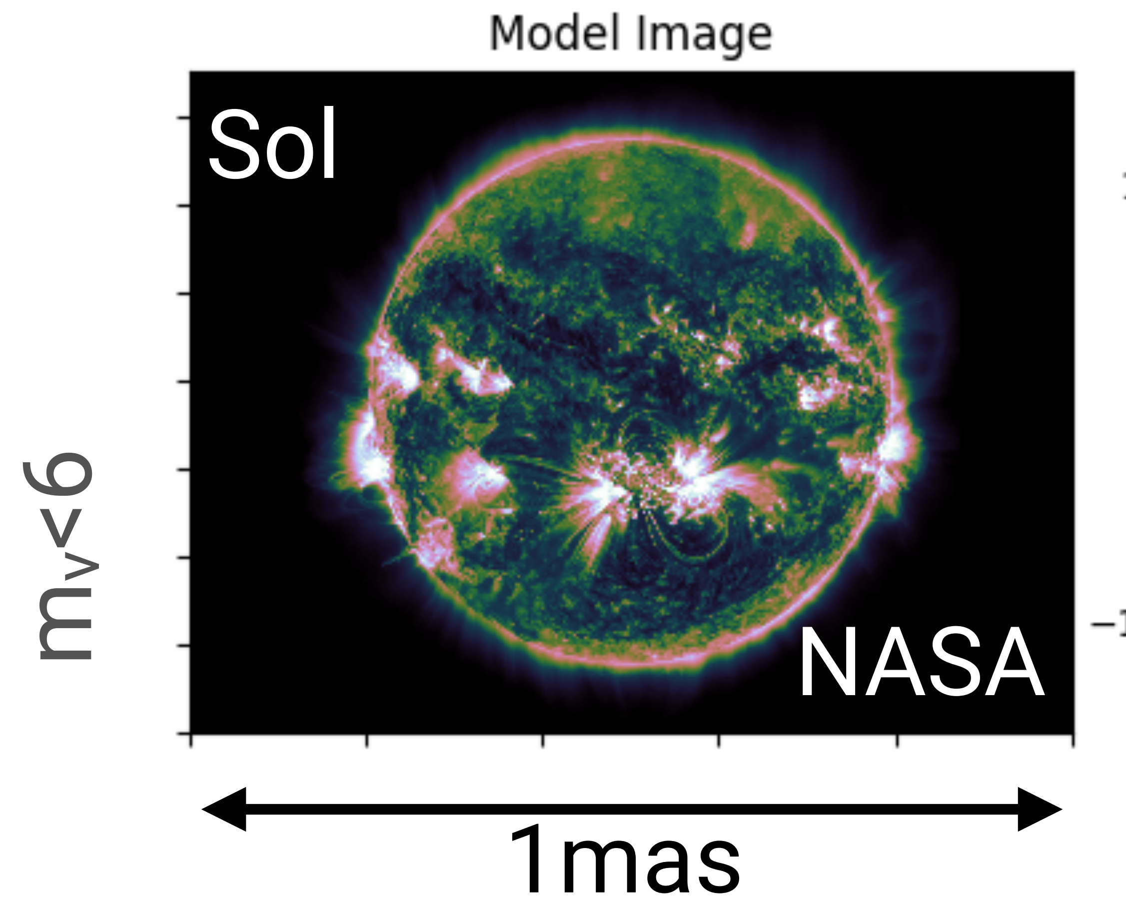

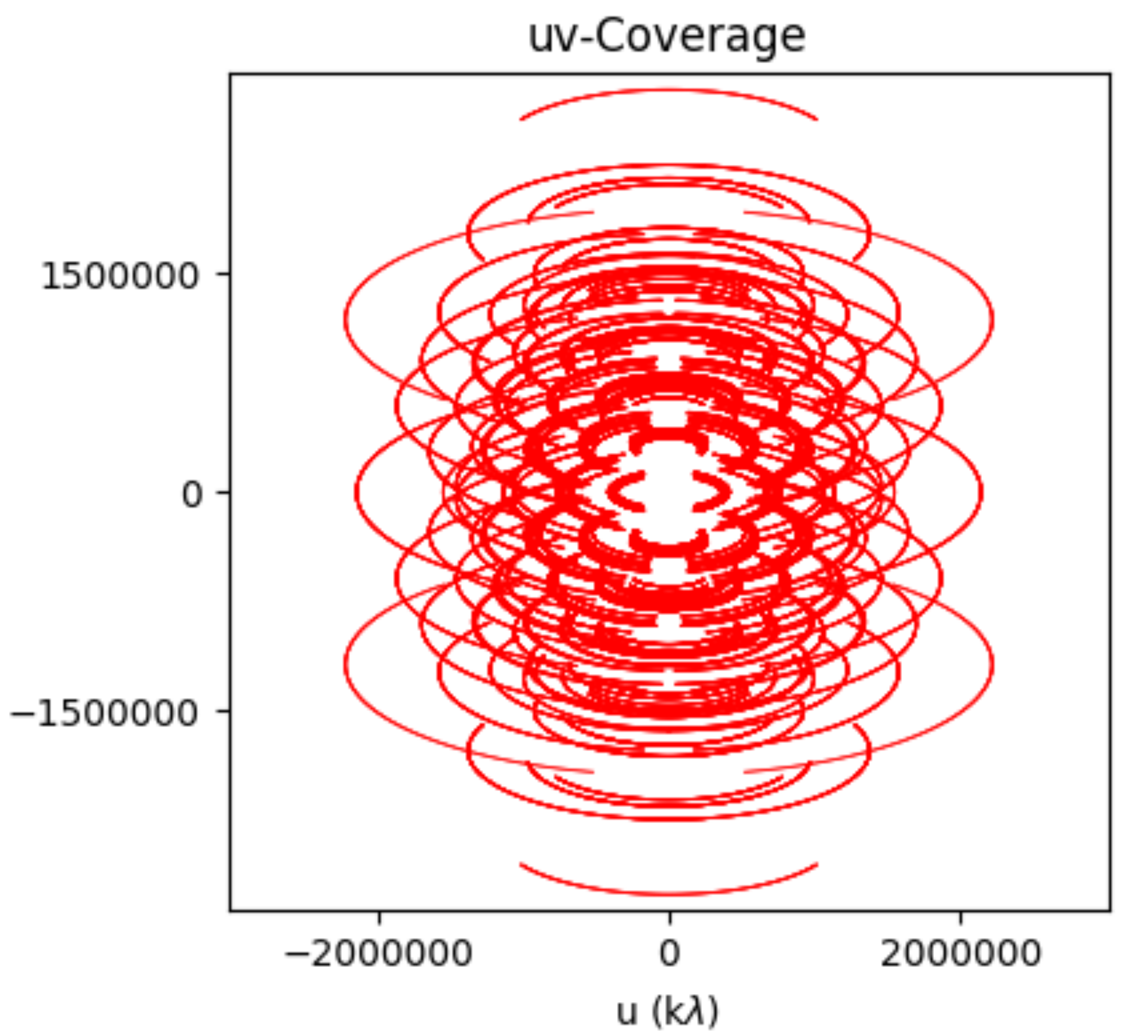

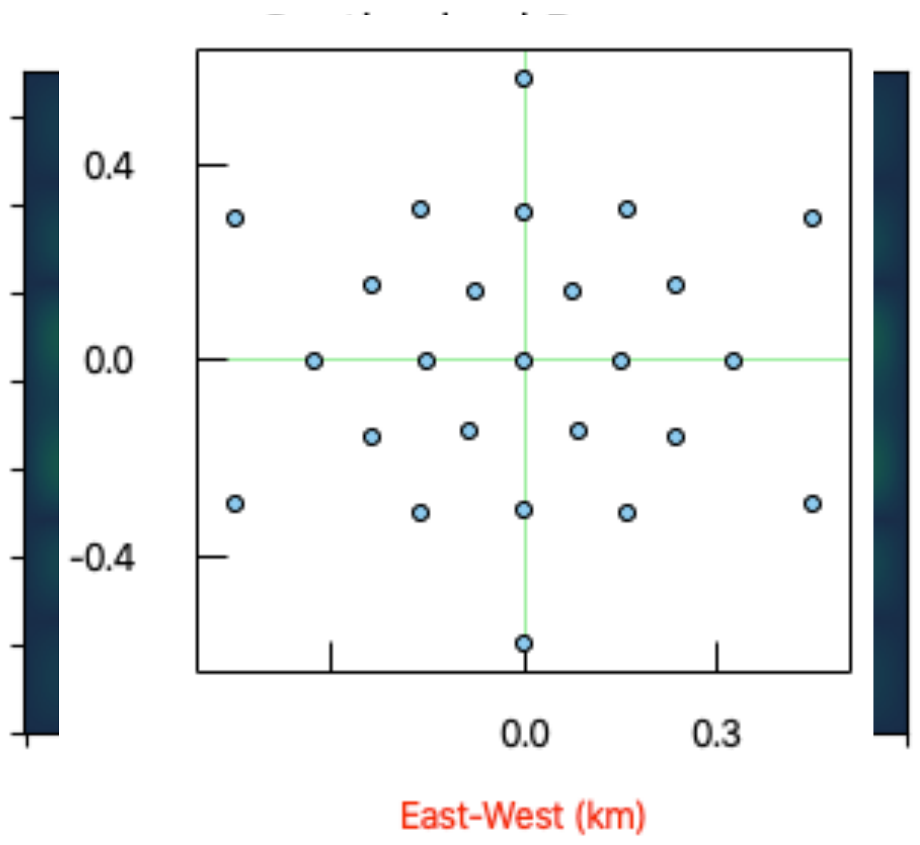

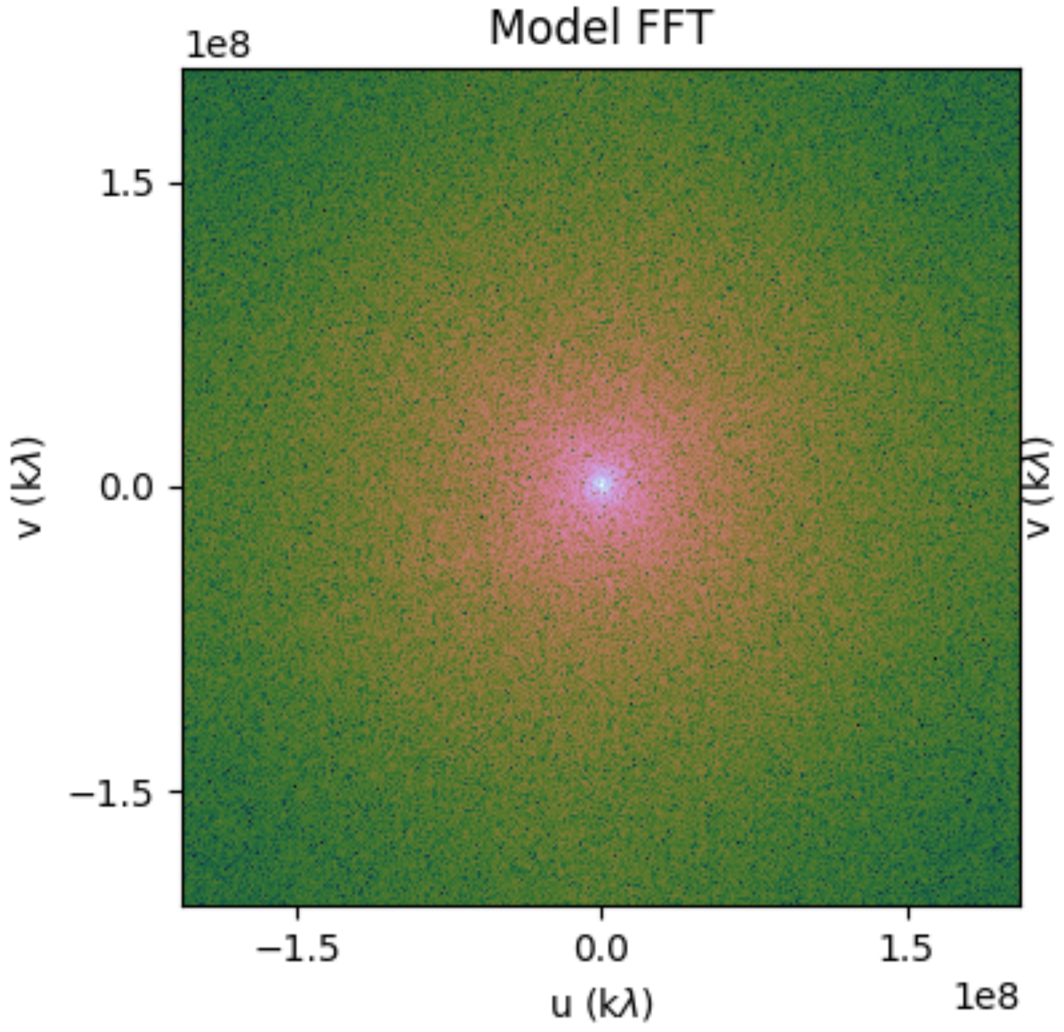

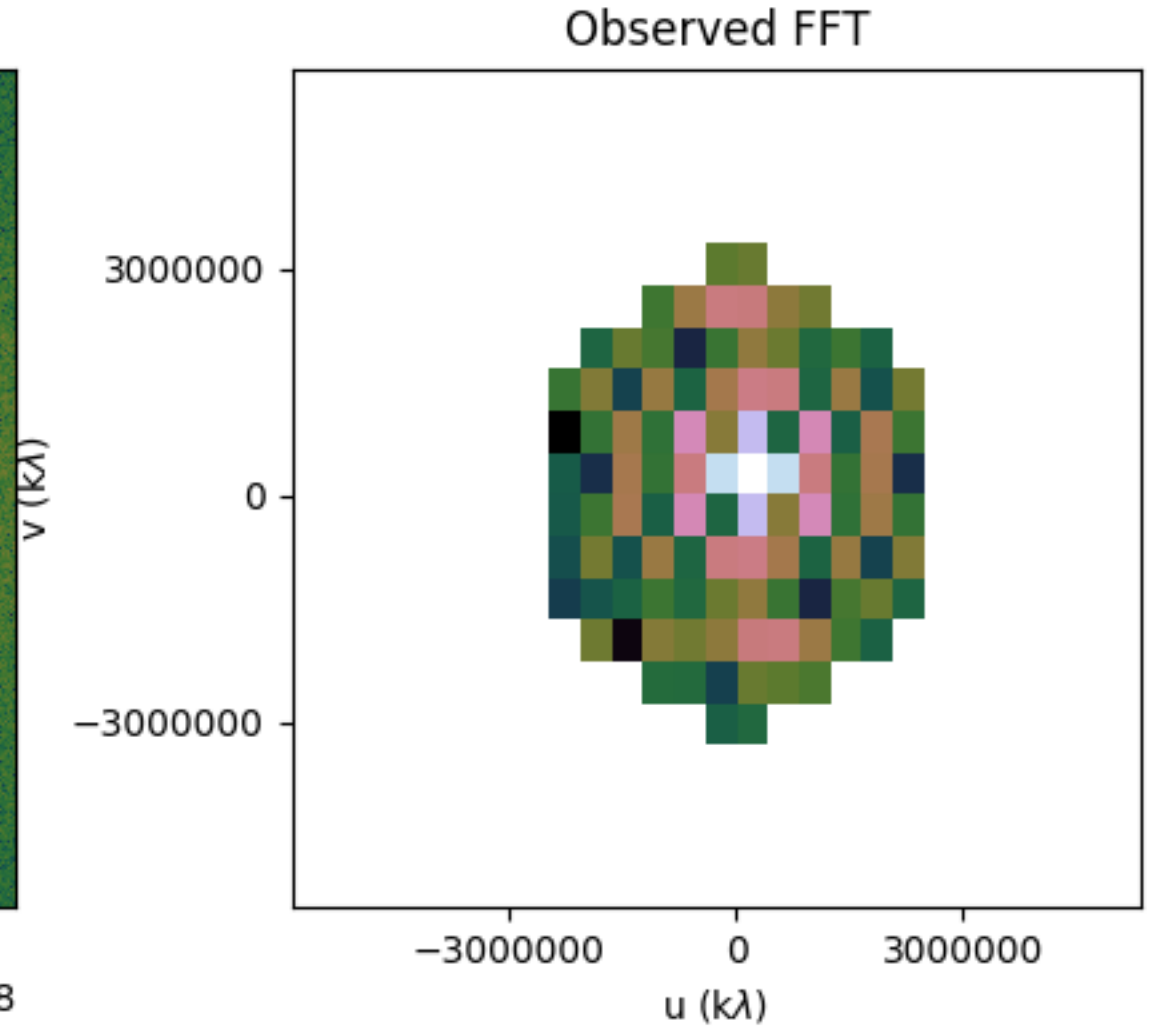

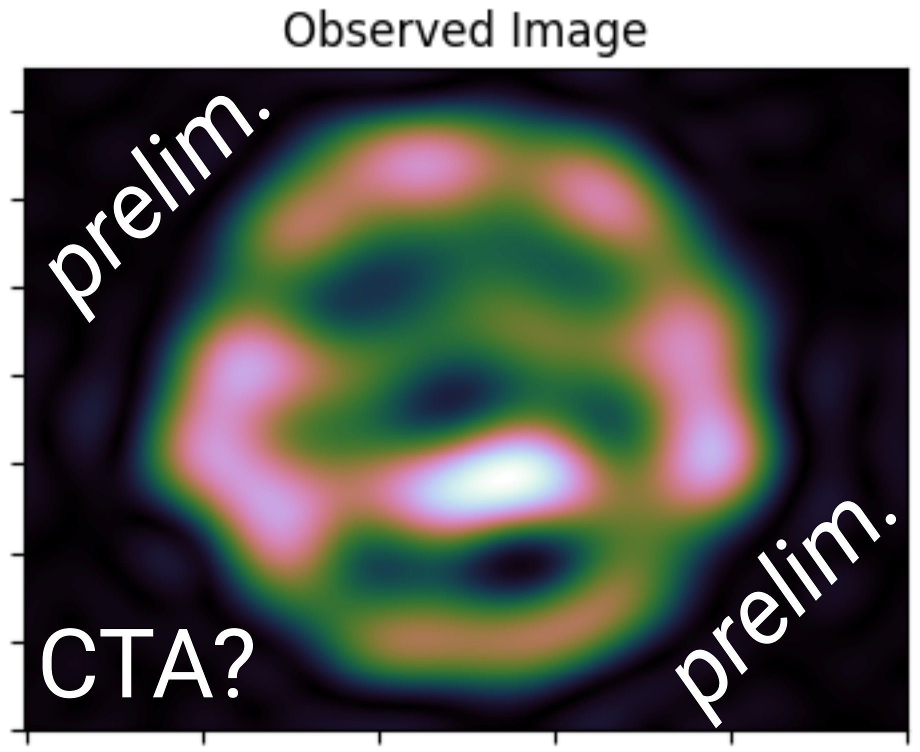

To do:

- estimate noise
- phase recovery methods

*** FFT sampling effects only ***

Simulation adapted from the friendlyVRI
https://crpurcell.github.io/friendlyVRI/

2h observation with CTA-S SSTs for a <1mas “solar-like” star at -20° declination

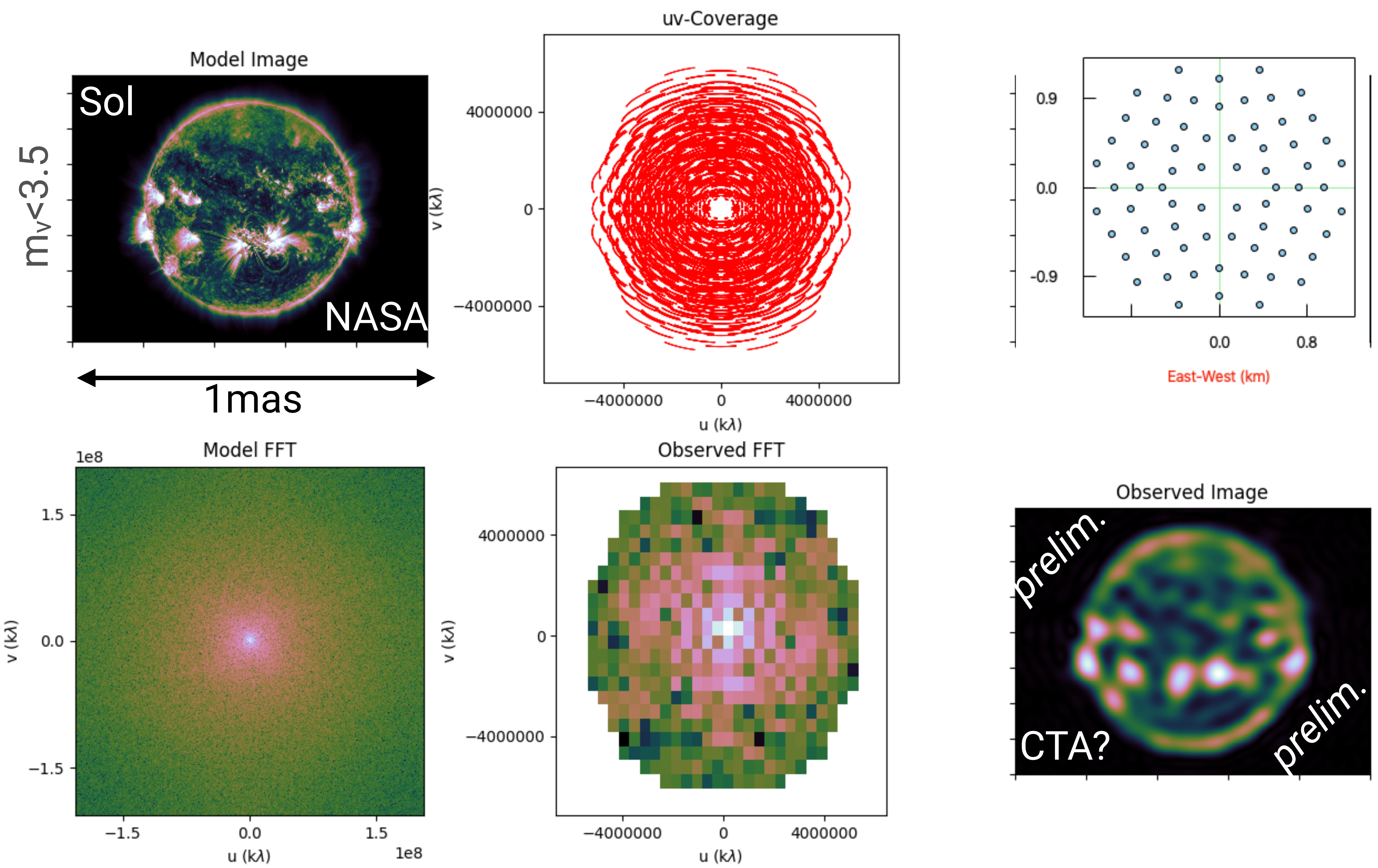

To do:
- estimate noise
- phase recovery methods
- **Count the star spots**

*** FFT sampling effects only ***

Simulation adapted from the friendlyVRI
https://crpurcell.github.io/friendlyVRI/

Remember these are never before achieved angular resolutions in the optical — we know that there are interesting things happening at these angular scales, but we can only predict some of what that might be…

η Carinae:
massive star, colliding wind binary, core collapse supernova / GRB progenitor

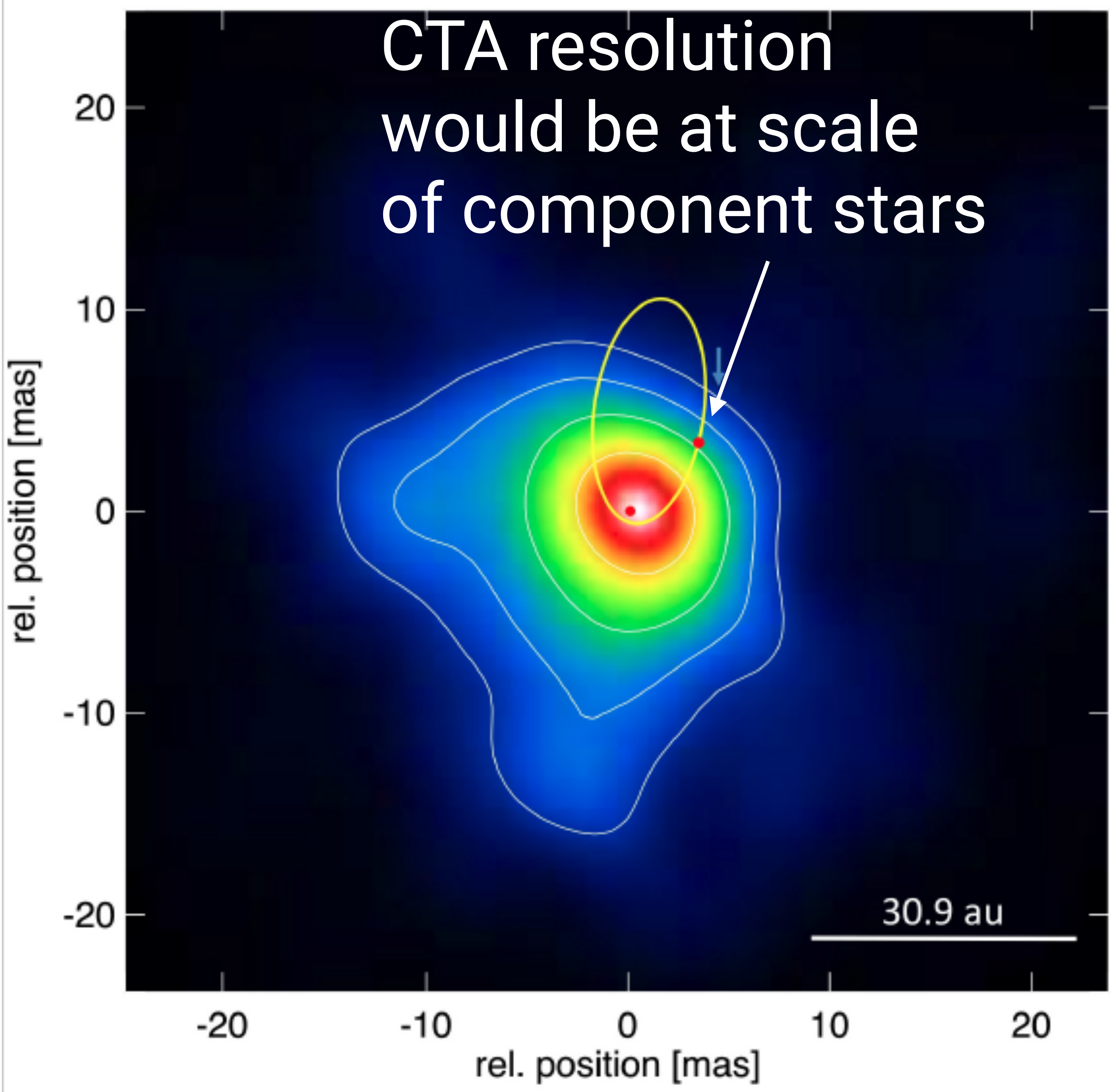

NB, II signal/noise is independent of spectral bandpass. Same resolution can be achieved in spectral lines not just continuum. Different wavelengths probe different optical depths

-> 3D imaging?

Weigelt et al. 'VLTI-AMBER velocity-resolved aperture synthesis imaging of η Carinae… Studies of the primary star wind and inner most wind-wind collision zone.'

A&A **594**, 106 (2016).

Come join the fun…

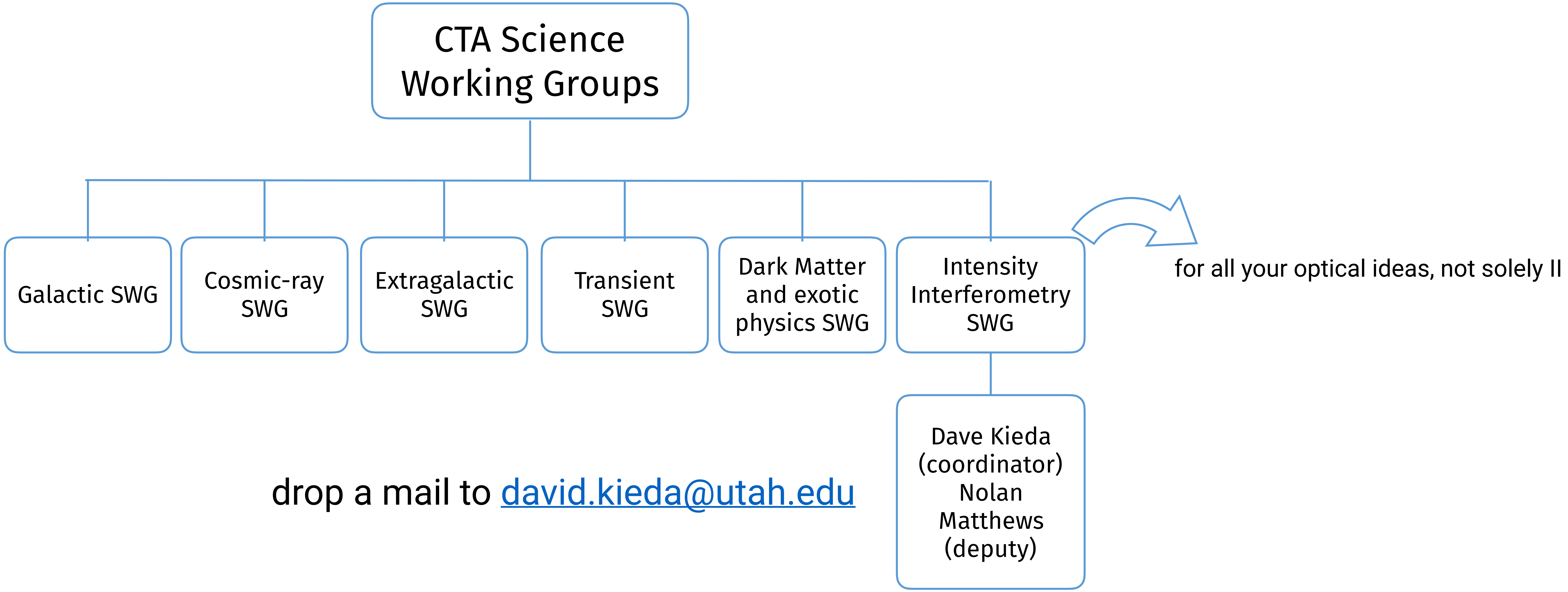

drop a mail to david.kieda@utah.edu

Summary

- Intensity Interferometry at sub-mas scale with IACTs has been achieved
  - clear signal on two stars (more to come)
  - it is an offline optical interferometer
    - can be scaled to arbitrary number of telescopes
      - simple to add new telescopes with commercial fibre optics
- CTA has imaging capability to <100µas resolution for hot, bright stars
  - angular diameters
  - limb darkening
  - rapid rotators
  - binary systems
  - emission line regions
  - star spots
  - …

Backup

CENTER FOR ASTROPHYSICS
HARVARD & SMITHSONIAN

Signal/Noise

$$(S/N)_{\mathrm{RMS}} = A \cdot \alpha \cdot n \cdot |\gamma_{12}(d)|^2 \cdot \sqrt{\Delta f \cdot T/2}$$

mirror area

photon detection efficiency

correlation

electronics bandwidth

observation time

photons/m^2/s/Hz

α = 0.35
cf NSII

Dish [m]	250 MHz	1 GHz
4	~0.5	~1
12	~5	~10
23	~20	~40

LeBohec & Holder *ApJ* **649**, 399 (2006)
$|\gamma_{12}|^2$=0.5 at 5σ to 14% accuracy in 5h for m_V=6.7
(3% for m_V=5)

Sensitivity

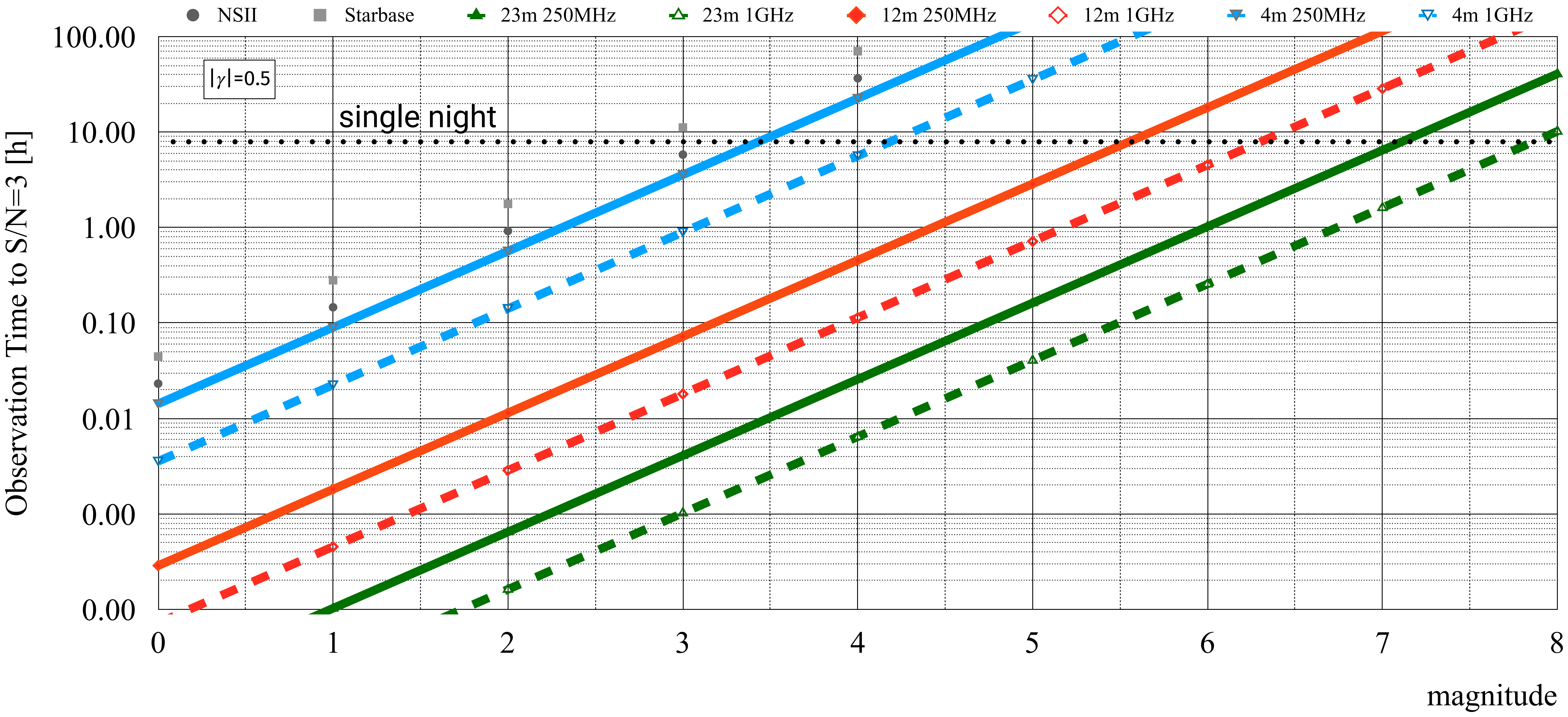

CENTER FOR ASTROPHYSICS
HARVARD & SMITHSONIAN

Table 2: Candidate sources from The Bright Star Catalogue: 35 stars brighter than $m_V = 2$ *or* hotter than $T_{eff} = 25{,}000$ K. Those whose angular diameters were measured already with the NSII [28] are marked with an asterisk (*).

Name	HR	θ [mas]	V_{rot} [km s^{-1}]	Spectral Type	T_{eff} [K]	m_V	Notes
Achernar, α Eri	472	1.9	250	B3 Ve	15 000	0.46	High V_{rot}, *
Rigel, β Ori	1713	2.4	30	B8 Iab	9 800	0.12	Emission-line star, *
λ Lep	1756		70	B0.5 IV	28 000	4.29	
Bellatrix, γ Ori	1790	0.7	60	B2 III	21 300	1.64	Variable, *
Elnath, β Tau = γ Aur [sic]	1791	1.5	70	B7 III	13 500	1.65	Binary system
υ Ori	1855		20	B0 V	28 000	4.62	Variable
HD 36960	1887		40	B0.5 V	26 000	4.78	Binary system
Alnilam, ϵ Ori	1903	0.7	90	B0 Iab	18 000	1.7	Emission-line star, *
μ Col	1996		150	O9.5 V	33 000	5.17	
β CMa	2294	0.5	35	B1 II-III	23 000	1.98	β Cep-type variable, *
Alhena, γ Gem	2421	1.4	30	A0 IV	9 100	1.93	*
S Mon	2456		60	O7 Ve	26 000	4.66	Pre-main-sequence
Sirius, α CMa	2491	5.9	10	A1 V	9 100	−1.46	*
EZ CMa	2583			WN4	33 000	6.91	Highly variable W-R star
Adara, ϵ CMa	2618	0.8	40	B2 Iab	20 000	1.5	Binary, *
Naos, ζ Pup	3165	0.4	210	O5 Ia	28 000	2.25	BY Dra variable, *
γ^2 Vel	3207	0.4		WC8 O7.5	50 000 35 000	1.78	Wolf-Rayet binary, *
β Car	3685	1.5	130	A2 IV	9 100	1.68	*
Regulus, α Leo	3982	1.4	330	B7 V	12 000	1.35	High V_{rot}, *
η Car	4210	5.0		peculiar	36 000	6.21	Extreme object, variable
Acrux, α^1 Cru	4730		120	B0.5 IV	24 000	1.33	Close binary to α^2 Cru
Acrux, α^2 Cru	4731		200	B1 V	28 000	1.73	Close binary to α^1 Cru
β Cru	4853	0.7	40	B0.5 IV	23 000	1.25	β Cep-type variable, *
ϵ UMa	4905		40	A0 p	9 500	1.77	α^2 CVn-type variable
Spica, α Vir	5056	0.9	160	B1 III-IV	23 000	0.98	β Cep-type variable
Alkaid, η UMa	5191	< 2	200	B3 V	18 000	1.86	Variable
β Cen	5267	0.9	140	B1 III	23 000	0.61	β Cep-type variable
τ Sco	6165		25	B0.2 V	26 000	2.82	
λ Sco	6527		160	B2 IV+	21 000	1.63	β Cep-type variable
Kaus Australis, ϵ Sgr	6879	1.4	140	B9.5 III	9 800	1.85	Binary, *
Vega, α Lyr	7001	3.2	15	A0 V	9 100	0.03	*
Peacock, α Pav	7790	0.8	40	B2 IV	19 000	1.94	Spectroscopic binary, *
Deneb, α Cyg	7924	2.2	20	A2 Iae	9 300	1.25	Variable
α Gru	8425	1.0	230	B6 V	13 000	1.74	*
Fomalhaut, α PsA	8728	2	100	A4 V	9 300	1.16	With imaged exoplanet, *

Dravins et al *NewAR* **56**, 143 (2012).
Dravins et al *APh* **43**, 331 (2013).

Table 5. Main-sequence stars, according to their spectral type (top) and apparent magnitude (bottom), observable from Kitt Peak.

Spectral type	Number of fully resolved stars	Overlap with CHARA	Number of partially resolved stars
M	230	230	0
K	729	726	0
G	424	282	0
F	431	118	52
A	364	77	348
B	205	44	328
O	4	0	6
Total	2387	1450	734
Apparent magnitude	**Number of fully resolved stars**	**Number of partially resolved stars**	**Approximate integration time[a]**
≤ 1	7	0	$\ll$1h
1 to 2	18	0	$\ll$1h
2 to 3	76	0	$\ll$1h
3 to 4	199	5	0.2 h
4 to 5	667	52	1.24 h
5 to 6	1420	677	8 h
Total	2387	734	

Note. [a]In order to obtain angular size measurement with a precision of ~10 per cent.

SPIIFy
Pilyavsky et al. *MNRAS* **467**, 3048 (2017)

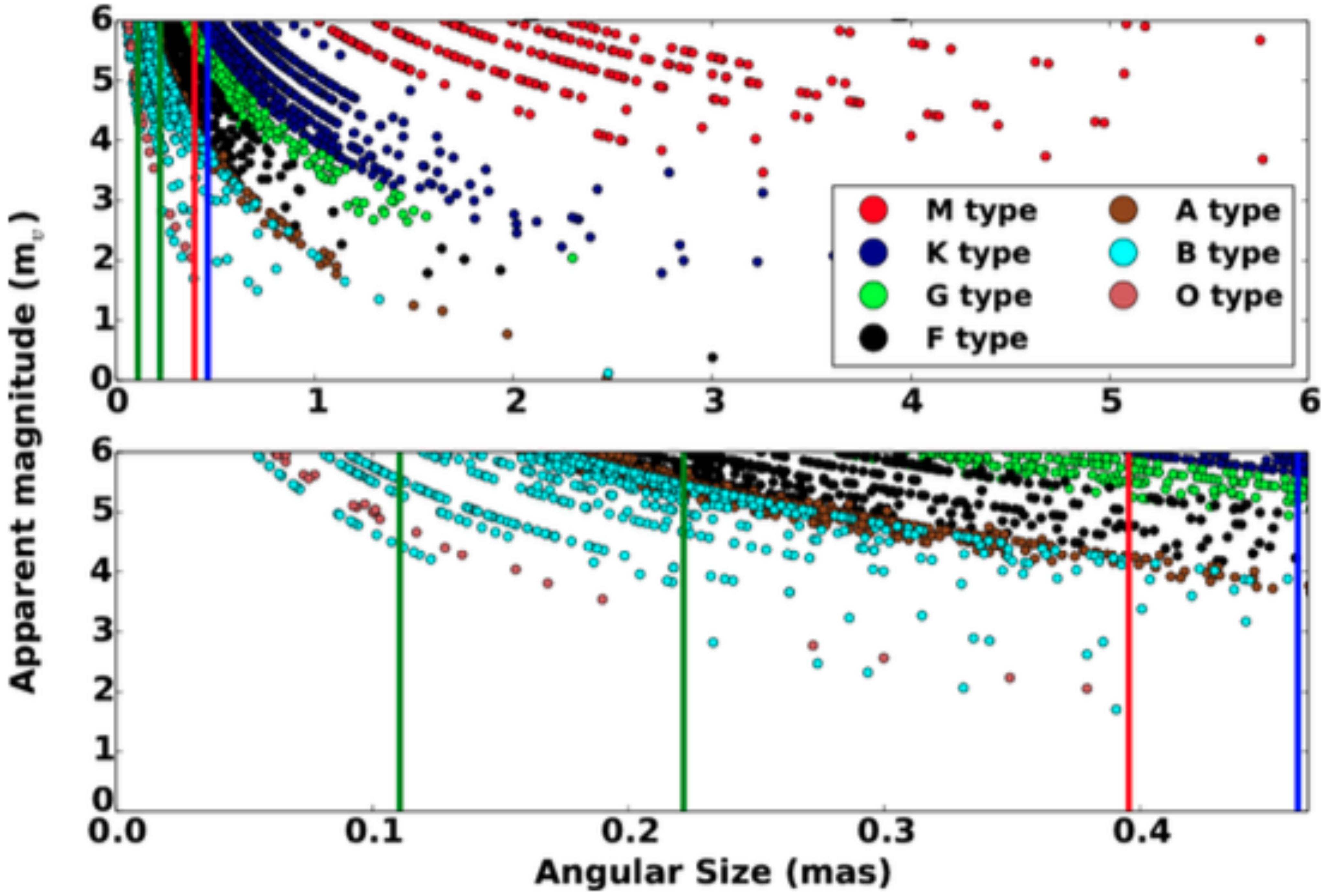

Figure 6. Top: stellar magnitudes from the Bright Star Catalogue plotted as a function of their approximate angular size. The colours correspond to the spectral type, given in the legend. Bottom: identical plot, with a narrower range in angular size, showing the bounds where observations from Kitt Peak can fully resolve the star (~0.21 milliarcsec) and bounds where stars will be partially resolved (~0.11 milliarcsec).

SPIIFy
Pilyavsky et al. *MNRAS* **467**, 3048 (2017)

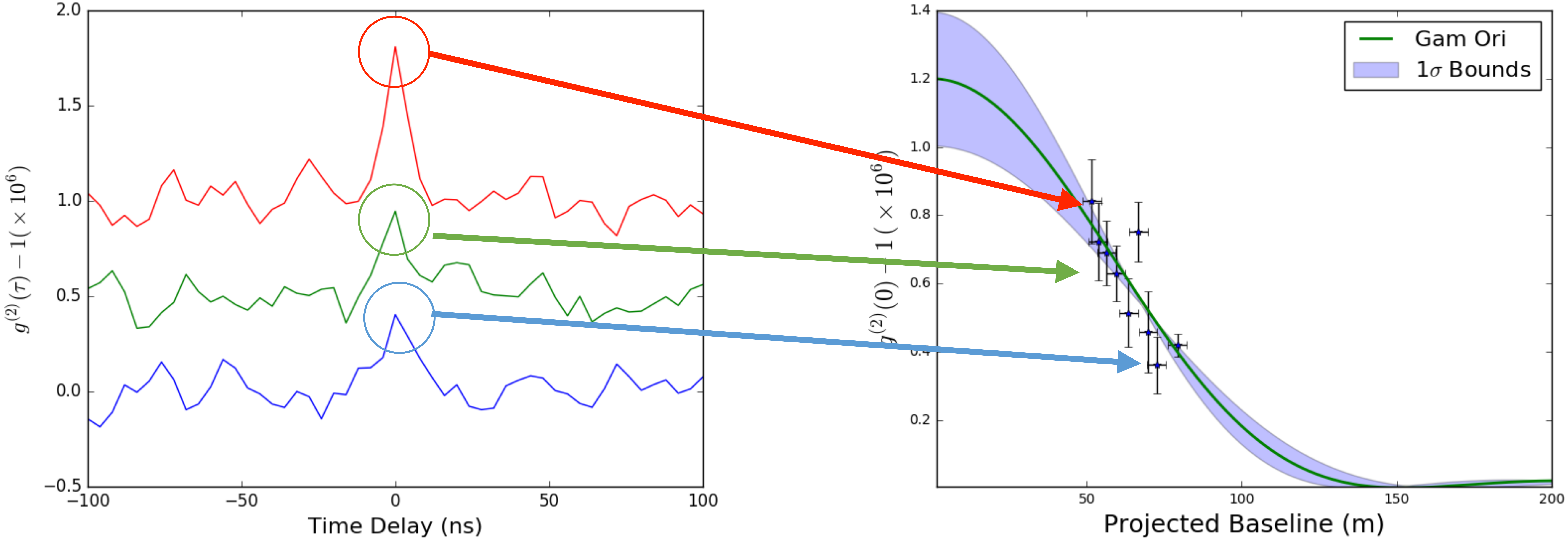

2.0
1.5
1.0
0.5
0.0
−0.5
−100
−50
0
50
100
$g^{(2)}(\tau) - 1(\times 10^6)$
Time Delay (ns)
1.4
1.2
1.0
0.8
0.6
0.4
0.2
50
100
150
200
$g^{(2)}(0) - 1(\times 10^6)$
Projected Baseline (m)
Gam Ori
1σ Bounds

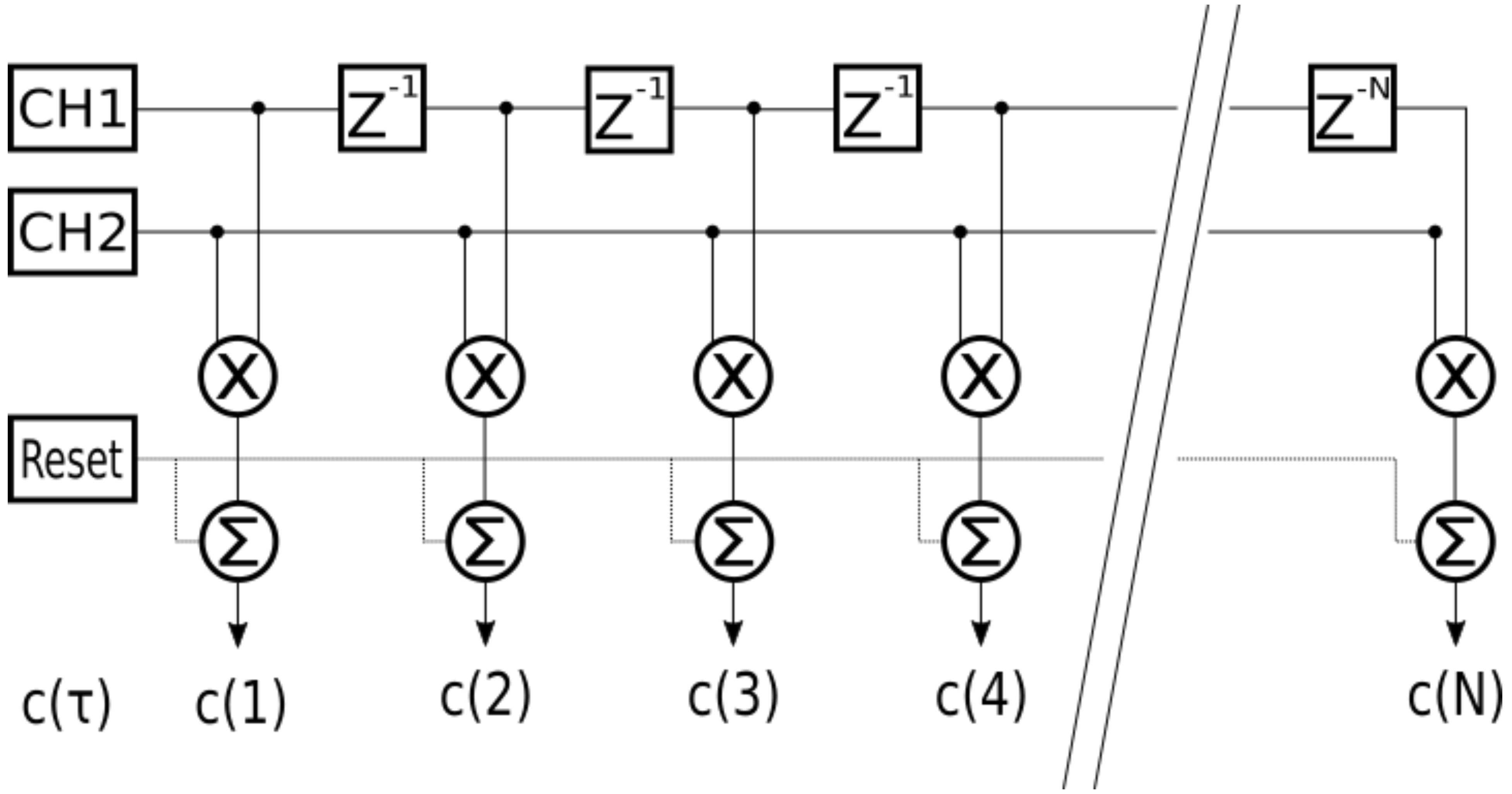

- Virtex-5 FPGA programmed to perform high-speed correlations of real-time/streamed data
  - Based on a multiply-accumulate algorithm
  - (Currently) performs correlation for 64 time-lag bins (-128 to +128ns in 4ns steps)

- Allows for rapid processing of large data sets:
  - Single night of observations generates ~20TB
  - ~1:1 observation/computing time processing (allows data to be processed before the next night)

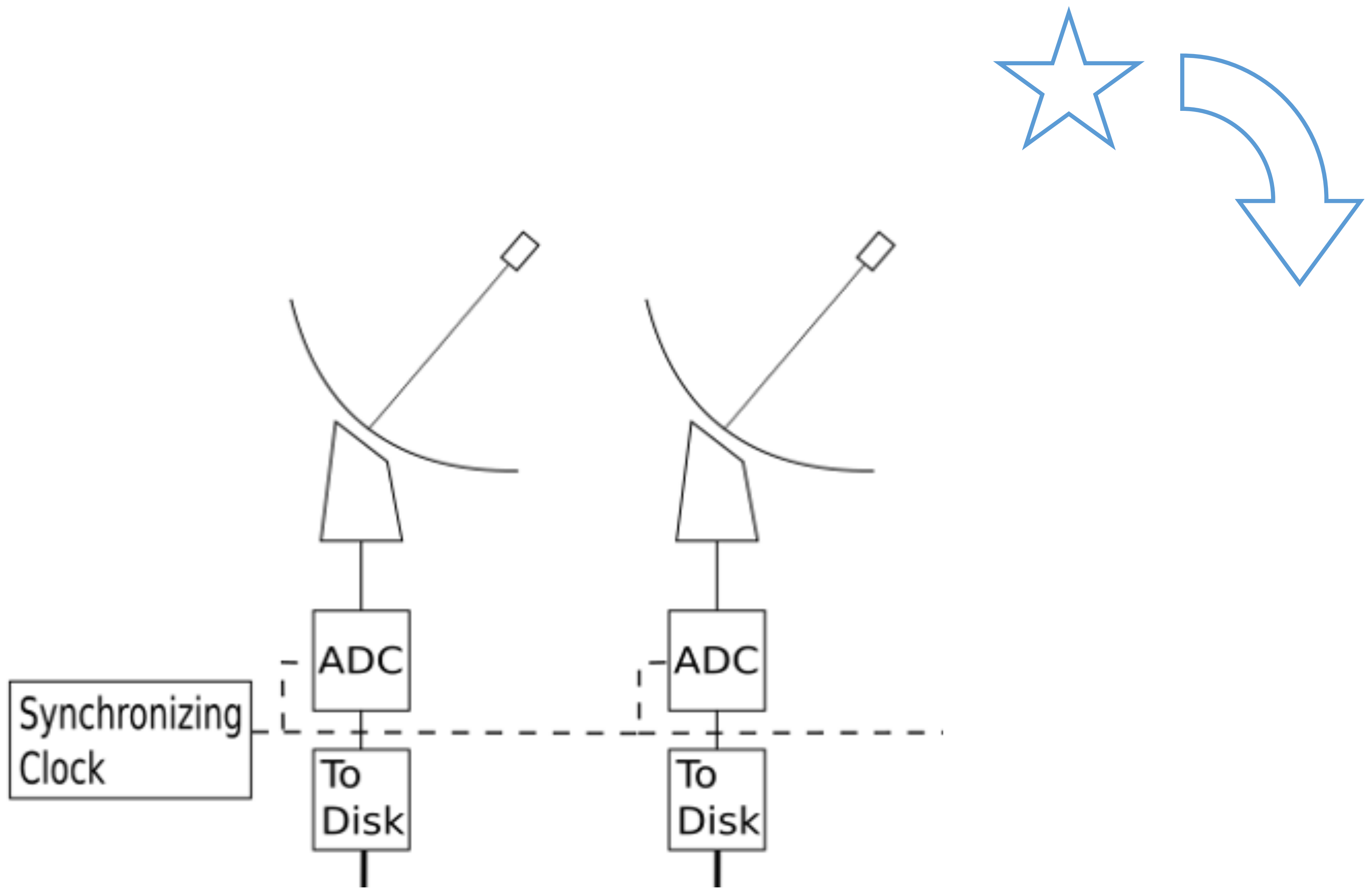

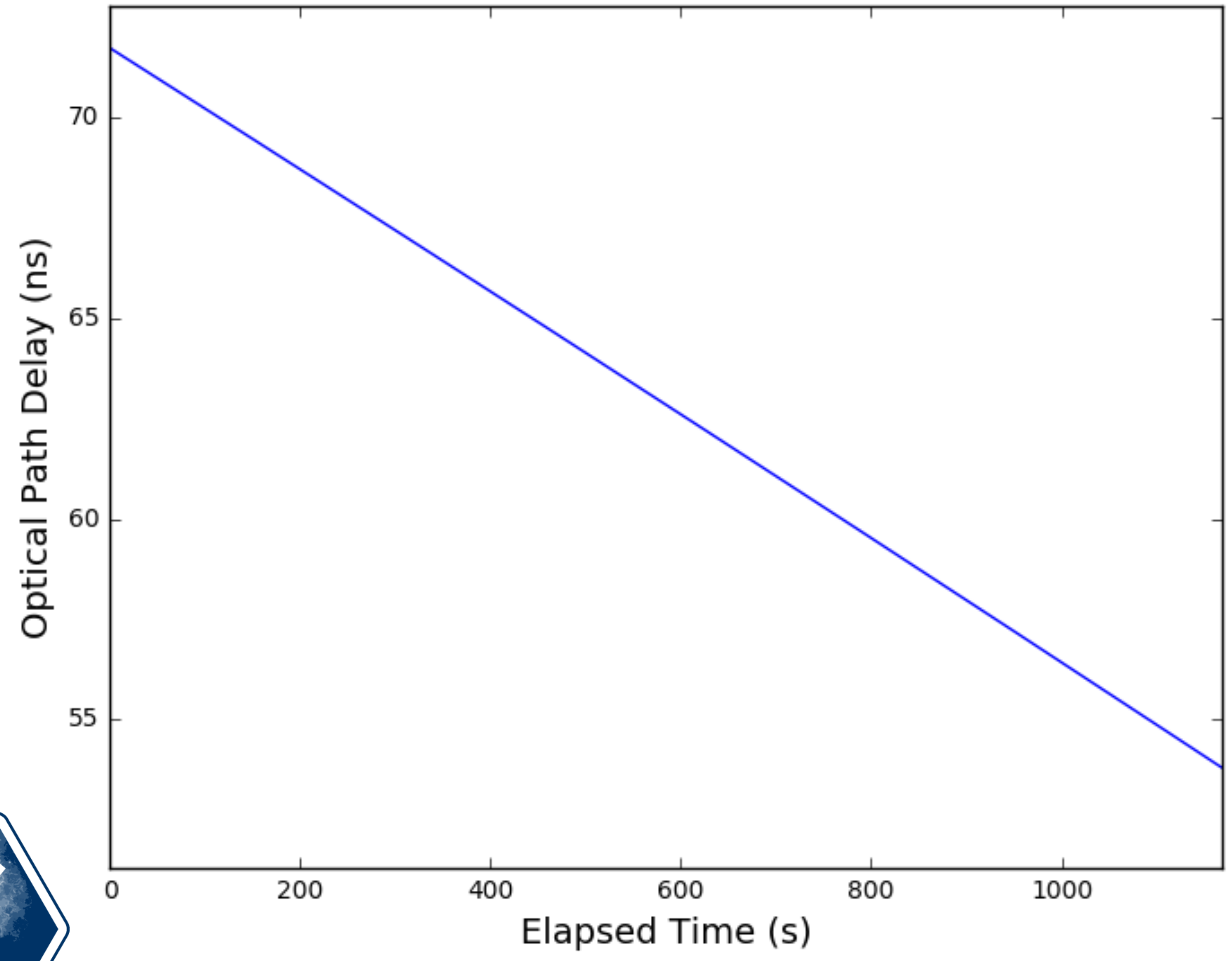

- The desired spatial coherence signal appears at the correlator time-lag that is equal to the geometric optical path delay (OPD).

- The OPD continuously changes on short time scales (~mins) by an amount > than the sampling time
  - Effect is signal moves across multiple time-lag bins

- To account for this the correlator is read out at a ‘cycle’ rate (~1s) in which OPD change relative to sampling time is negligible

- Software time correction applied aligning each correlator cycle output about known OPD for each respective cycle